



1 **Enhanced Evaluation of Sub-daily and Daily Extreme** 2 **Precipitation in Norway from Convection-Permitting Models at** 3 **Regional and Local Scales**

4

5 Kun Xie^{1,2}, Lu Li³, Hua Chen^{1,2}, Stephanie Mayer³, Andreas Dobler⁴, Chong-Yu Xu⁵, Ozan Mert
6 Gokturk³

7

8 ¹State Key Laboratory of Water Resources and Hydropower Engineering Science, Wuhan University, Wuhan

9 430072, P. R. China

10 ²Hubei Provincial Key Lab of Water System Science for Sponge City Construction, Wuhan University, Wuhan,

11 China

12 ³NORCE Norwegian Research Centre, Bjerknes Centre for Climate Research, Bergen, Norway

13 ⁴The Norwegian Meteorological Institute, Oslo, Norway

14 ⁵Department of Geosciences, University of Oslo, P.O Box 1047 Blindern, 0316 Oslo, Norway

15

16 *Correspondence to:* Hua Chen (chua@whu.edu.cn); Lu Li (luli@norceresearch.no)

17 **Abstract**

18 Convection-permitting regional climate models (CPRCMs) have demonstrated enhanced capability in capturing
19 extreme precipitation compared to regional climate models (RCMs) with convection-parameterization schemes.
20 Despite this, a comprehensive understanding of their added values in daily or sub-daily extremes, especially at local
21 scale, remains limited. In this study, we conduct a thorough comparison of daily and sub-daily extreme precipitation
22 from HARMONIE-Climate model, cycle 38 at 3km resolution (HCLIM3) and 12km resolution (HCLIM12) across
23 Norway's diverse landscape, divided into eight regions, using both gridded and in-situ observations. Our main focus
24 is to investigate the added value of CPRCMs (i.e., HCLIM3) compared to RCMs (i.e., HCLIM12) for extreme
25 precipitation at daily and sub-daily scales from regional to local scales, and quantify to what extend CPRCM can
26 reproduce the orographic effect on extreme precipitation at daily and sub-daily scale. We find that HCLIM3 better
27 matches observations than HCLIM12 for daily and sub-daily precipitation extreme indices at regional scale in
28 Norway. More specifically, HCLIM3 better captures the maximum 1-day precipitation (Rx1d) at most of the regions
29 except south-western region in Norway. Notably, HCLIM12 shows underestimation in the complex orography for
30 annual Rx1d. For the maximum 1-hour precipitation (Rx1h), the superiority from HCLIM3 have also been found on
31 average, although with slightly higher wet-bias in the western, middle-inland and middle-coastal during summer. In
32 addition, the reverse orography effect on seasonal Rx1h at regional scale can be better reproduced by HCLIM3 than



33 HCLIM12 in most seasons except spring. At the local scale, HCLIM3 can better capture the temporal evolution of
34 Rx1h than HCLIM12 when compared with observations between 1999-2018. However, we see that the benefit from
35 HCLIM3 in capturing seasonal Rx1d within western region diminishes at local scale. Most interesting finding is that
36 the added value from HCLIM3 is clearer in Rx1h than in Rx1d at both regional and local scale, especially in the
37 extreme seasonality. In general, HCLIM3 performs better than HCLIM12 on Rx1d and Rx1h in Norway with the
38 mean of bias distribution closer to zero, although it varies a bit among regions. Specifically, HCLIM3 performs
39 slightly poorer in the south-western region. This study highlights the importance of more realistic convection-
40 permitting regional climate simulations in providing reliable insights into the characteristics of precipitation
41 extremes across Norway's eight regions. Such information is crucial for effective adaptation management to mitigate
42 severe hydro-meteorological hazards, especially for the local extremes.

43 **1 Introduction**

44 In recent years, the world has witnessed a surge in both frequency and intensity of floods primarily attributed to the
45 increasing occurrence of intensive rainfall events (Tabari, 2020). These changes underscore the pressing need to
46 develop a predictive understanding of precipitation extremes for the upcoming decades, given the ongoing globe
47 warming. The intensification of precipitation extremes under the influence of global warming has the potential to
48 trigger severe natural hazards and exert significant socioeconomic impacts (Thackeray et al., 2022), which has
49 gained substantial attention in recent research endeavors. However, most of the previous research in this domain
50 have been based on the utilization of coarse resolution GCMs with grid sizes exceeding 100 km which have fallen
51 short in accurately simulating extreme precipitation events and its frequency due to their coarser resolution (Piani et
52 al., 2010; Wang et al., 2017). Notably, these GCMs tend to produce the largest errors in predicting extreme
53 precipitation, particularly in cases involving heavier convective activity, as observed in the study by Gervais et al.
54 (2014a). Despite various bias-correction techniques are applied to mitigate these discrepancies on the GCMs, as well
55 as employing them as forcing data for regional climate models (RCMs) with grid size larger than 10 km, it remains a
56 persistent challenge to eliminate the transfer of biases from GCMs to RCMs, as noted by studies such as
57 Pontoppidan et al. (2018) and Kim et al. (2020). The large resolution gap between GCMs or RCMs and localized
58 precipitation extremes further constrains the robust simulations of extreme precipitation as highlighted by Li et al.
59 (2020a). In addition, the reliance on parameterization schemes to represent convection in these coarse resolution
60 models introduces a significant source of uncertainty in modelling errors (Prein et al., 2015; Kendon et al., 2019).
61 More frequent and intense precipitation events under global warming stimulate interest in higher resolution and
62 physics-based models to improve the estimates of short-duration extremes.

63 Convection-permitting regional climate models (CPRCMs), with grid size of less than 4 km, offer a promising
64 alternative, which explicitly represent convection, eliminating the need for parameterizations of atmospheric deep
65 convection. The potential in resolving deep convection and local extremes from CPRCMs lead to the realistic
66 representation in daily and sub-daily precipitation features, including diurnal cycle, intensity and frequency of heavy
67 precipitation events, seasonality, spatial-temporal pattern, wet-spell and dry-spell. For instance, CPRCMs have been



68 proven to reduce the bias and enhance the representation in precipitation intensity and intensity in the Tibetan
69 Plateau, the highest highland in the world, as shown in Li et al. (2021). In addition to their capability in capturing
70 precipitation, Liu et al. (2017) also demonstrated the confidence of CPRCMs in estimating snowfall and snowpack
71 in the central U.S. Furthermore, the importance of CPRCMs in representing dry spell, dry and wet extremes induced
72 by local convective activity across Africa has also been found in Kendon et al. (2019), Chapman et al. (2023) further
73 confirmed its benefit in capturing rare rainfall extreme and local feature. In UK, Kendon et al. (2023) and Kent et al.
74 (2022) have found the benefit of CPRCMs compared to RCMs with convection parameterization schemes.
75 Additionally, the superior performance in capturing hourly and daily extreme precipitation including return-level,
76 frequency and intensity from CPRCMs over Alpine in Europe, has also been highlighted by Adinolfi et al. (2021),
77 Dallan et al. (2023) and Giordani et al. (2023).

78 Northern Europe has been reported to experience the most increase in precipitation, as indicated by Dyrddal et
79 al., (2023), where a novel CPRCMs have been developed within the Nordic Convection Permitting Climate
80 Projections project (NorCP) based on the convection-permitting HARMONIE-Climate model, cycle 38 (HCLIM38)
81 at a resolution of 3 km (HCLIM3) and 12km (HCLIM12). Through comparisons of seasonal precipitation, daily
82 mean precipitation, higher-intensity daily precipitation, the diurnal of hourly precipitation including frequency and
83 intensity from HCLIM3 and HCLIM12 over Fenno-Scandinavia, Lind et al. (2020) emphasized the add-value of
84 CPRCM in reproducing extreme precipitation, primarily over complex terrain, compared to coarser-scale model.
85 Médus et al. (2022) also noted that the summer diurnal cycle of frequency and intensity of hourly precipitation was
86 correctly captured in HCLIM3 compared to HCLIM12 in the Nordic region, with HCLIM12 underestimating the
87 diurnal cycle. However, the evaluation and conclusions from Lind et al. (2020) and Médus et al. (2022) were mainly
88 focused on the large regional and country scale of Fenno-Scandinavia, overlooking the added values of CPRCM at
89 local scale. Furthermore, Thomassen et al. (2023) observed that HCLIM3 tends to exhibit underestimations in
90 monthly precipitation and a later evening peak compared to sub-kilometre models. They found that the advantages
91 of sub-kilometer models were not outstanding. These evaluations were based on gridded datasets, which introduce
92 uncertainty at the local scale, especially over complex orography (Lussana et al., 2019). As Chapman et al. (2023)
93 demonstrated, who underscored the importance of assessing rare extreme rainfall events in eastern African using
94 convection-permitting models and parameterization convection models at both grid and station scales, that the
95 extreme from grids representing rainfall averaged over a larger area are damped and hence the return-level will be
96 smaller than observation. They found that the station-derived shape parameters and return levels are aligned with
97 observations, and suggested the significance of site-specific analysis and evaluations. The error induced by station
98 density in gridded dataset has also been indicated in Gervais et al. (2014b), who suggested the source of large errors
99 in gridded dataset when station density is low. Consequently, a comprehensive evaluation and analysis of the added
100 value from CPRCMs compared with RCMs that incorporates both regional and local scales is crucial for extreme
101 precipitations.

102 We acknowledge that Norway, a Nordic country, is representative of diverse climate features due to its
103 extended latitude, rugged coastline, plateaus, and complex orography. The dominances of precipitation between the



104 coastal and inland regions over Norway are distinctly different, and most of studies focusing on the hydrology and
105 meteorology over Norway were based on the divided regions (Vormoor et al., 2016; Poujol et al., 2021; Konstali
106 and Sorteberg, 2022). By dividing region with its characteristics, a more thorough comprehension of add-value of
107 CPRCM in capturing extreme precipitation can be reached. Therefore, reliable evaluation about analyzing the add-
108 value of CPRCM in capturing extreme precipitation should be scaled to region or local scale.

109 In the complex mountain areas, extreme precipitation is triggered by the interaction of large-scale atmospheric
110 activity and local orography property, which may cause severe hydrometeorological hazards, such as flash flooding.
111 However, understanding the orographic impact in precipitation in complex orography is challenging due to sparse
112 observations (Rossi et al., 2020). The poor representation of RCMs in capturing local precipitation have been
113 indicated in Knist et al. (2020). Importantly, CPRCMs shows superior in reproducing precipitation bias over higher
114 complex orography in the Alpine, as shown in Lind et al. (2016) and Reder et al. (2020). Furthermore, the better
115 representation of sub-daily and daily heavy precipitation from CPRCMs over the Alpine have also been found in
116 Ban et al. (2020) and Dallan et al. (2023). Marra et al. (2021) and Dallan et al. (2023) also confirmed the efficiency
117 of CPRCMs in reproducing the reverse orography effect on hourly extreme precipitation. Conversely, Rossi et al.
118 (2020) and Mahoney et al. (2015) found the weak depend of subdaily precipitation on elevation in the Colorado,
119 USA. Opposing the orographic enhance on daily precipitation, Dallan et al. (2023) indicated the no evident relation
120 of daily precipitation on elevation. It is worth noting that these ambiguous results were based on the annual maxima,
121 and the added value from CPRCMs than RCMs have not been explored. Moreover, the dependence on seasonality
122 for the performance of CPRCMs especially in complex orography need the evaluation based on season. Thus, we fill
123 this knowledge gap by characterizing orographic impact on hourly and daily extreme precipitation seasonally.

124 As highlighted by Konstali and Sorteberg (2022), there can be significant uncertainties associated with the
125 interpolation of grided precipitation data. Besides, the benefit for precipitation spatial evaluation based on in-situ
126 observation has also been reported in Thomassen et al. (2023). Therefore, the evaluation of extreme precipitation
127 from HCLIM3 and HCLIM12 here, is based on both grided precipitation and in-situ observation. Our study aims to
128 address the value of CPRCM (HCLIM3) in capturing the characteristics of extreme precipitation in Norway,
129 comparing it with a coarser resolution model (HCLIM12) as well as both of the in-situ and grided precipitation
130 observations. Here, our contribution to the existing literature, e.g., Médus et al. (2022), revolves around the added
131 value of CPRCM in the extreme precipitation characteristics, encompassing a range of metrics.

132 The main objectives of this study are (1) enhance understanding of convection-permitting climate models by
133 comparing their effectiveness in simulating extreme precipitation with that of regional climate models from regional
134 to local scales, highlighting the added value of CPRCMs; (2) assess HCLIM3's capability in depicting orographic
135 effects on seasonal extreme precipitation. This research explores whether the benefits provided by CPRCMs hold
136 consistently in different regions driven by varying physical processes for precipitation. Finally, our study delves into
137 the analysis of the intensity and frequency of extreme precipitation events, offering insights into local and regional
138 variations.

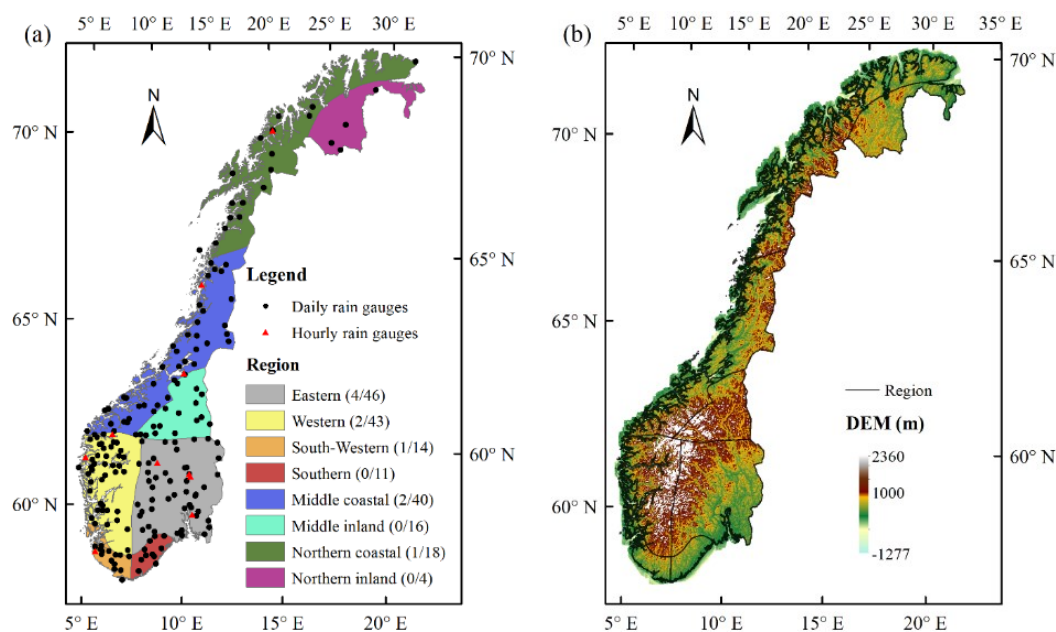


139 2 Study area and data

140 2.1 Study area

141

142



143

144 **Figure 1: (a) The division of 8 precipitation regions in Norway. In the legend, the numbers shown in the brackets after**
145 **each region represent the available size of hourly / daily stations in the region during 1999 – 2018. For example, Eastern**
146 **(4/46) means that there are available data from 4 hourly stations and 46 daily stations in the Eastern region during 1999–**
147 **2018; (b) Spatial distribution of topography over Norway.**

148

149 The different climate regimes between coastal and inland regions over Norway compels the analysis of hydro-
150 meteorology based on divided regions. We divided Norway into eight regions according to similar season cycle
151 characteristics (Michel et al., 2021): Eastern (E), Southern (S), South-Western (SW), Western (W), Middle-Inland
152 (MI), Middle-Coastal (MCo), Northern-Coastal (NCo), and Northern-Inland (NI), shown in Fig.1.

153

154 The study areas cover the mainland Norway which has unique climate characteristics within different regions.
155 The eastern region with stratiform precipitation originating from south and south-east is dominant by continental
156 climate, with convective precipitation in summer. Most of extreme events occurring in the western region with
157 abrupt topography are mainly related to atmospheric rivers (AR), peaking in winter. The wettest region strongest
158 affected by the North Atlantic storm track with enhanced precipitation from front systems and land-falling storms
159 due to the uplift over the Scandes (Poujol et al., 2021), is the west coast of Norway. For the middle-coastal and
160 northern coastal regions, 59% of extremes are associated with AR, and the precipitation rate decreases moving
161 inland (Konstali and Sorteberg, 2022). Northern-inland and middle-inland are the driest regions with lower wet-day
intensity (<6 mm/day) and wet-day frequency (<33%), most extremes during summer are linked to AR for the



162 northern-inland where largest precipitation is dominant by cyclones. South-western region lies at the end of the
163 climatological jet and is regularly hit by ARs especially during the Zonal and Atlantic Trough weather regimes
164 (Michel et al., 2021). The main precipitation in Norway is winter and autumn precipitation. These precipitation
165 patterns in spatial and seasonality are mainly linked to ARs (Schaller et al., 2020; Benedict et al., 2019).
166

167 2.2 Data

168 We utilize the outputs of double nesting from HCLIM38 model based on the ALADIN-HIRLAM NWP system,
169 which include different configuration settings for each spatial resolution: HCLIM3 and HCLIM12 with hydrostatic
170 dynamics. HCLIM12 covers over most part of Europe with 313×349 grid-points using the ERA-Interim reanalysis
171 ~ 80 km as boundary condition for every 6 h, and HCLIM3 spans over the Fenno-Scandinavia region with 637×853
172 horizontal grid-points using the HCLIM12 as boundary condition for every 3 h. Importantly, the convection-
173 parameterization scheme was switched-off in HCLIM3, allowing for an explicit representation of convection
174 processes. The present-day simulations from HCLIM3 and HCLIM12 span over the years 1997-2018. For more
175 comprehensive information, refer to the work of Lind et al. (2020) and Médus et al. (2022).

176 This study primarily centers on assessing the performance of HCLIM3 and HCLIM12 in simulating sub-daily
177 and daily extreme precipitation events in the present-day (1999-2018) in Norway mainland. The models' outputs are
178 specifically extracted for Norway mainland. Before analysis, HCLIM3 data was resample to the HCLIM12 grid
179 (12km) using a bilinear method.

180 seNorge2018 (SeNorge) covering Norway with 1-day temporal and 1 km spatial resolution (Lussana et al.,
181 2019) is used as the observation to evaluate the performance of HCLIM3 and HCLIM12 during 1999-2018.
182 SeNorge2 with 1-hour and 1 km spatial resolution is also applied to evaluate the hourly result during 2010-2018
183 (Lussana et al., 2018). In addition, in-situ observations including hourly and daily resolution are downloaded from
184 Norwegian Meteorological Institute [Frost API \(met.no\)](https://met.no).

185 3 Methods

186 3.1 Evaluation of precipitation

187 To evaluate the characteristics of precipitation extremes between HCLIM3 and HCLIM12, we compared the
188 historical simulations with daily SeNorge gridded dataset, hourly SeNorge2 gridded dataset and in-situ observations.
189 We only keep the stations that have less than 10% of the data missing during 1999-2018 and consider station
190 distribution uniformity, which give a total of 192 daily stations and 10 hourly stations, respectively, over Norway
191 (Fig. 1 and Table 1). In this study, the evaluation based on in-situ observation and gridded dataset (SeNorge and
192 Senorge2) was defined as the local scale and regional scale, respectively.

193 For the evaluation at regional scale, HCLIM3 and SeNorge, SeNorge2 were resampled to HCLIM12 grid ~ 12
194 km. Therefore, the observed and simulated extreme indices were calculated at grid scale, and then averaged the
195 extreme indices within the corresponding region. For the evaluation based on in-situ observation, HCLIM3 and



196 HCLIM12 were interpolated to the 192 daily rain-gauges and 10 hourly rain-gauges to calculate the indices using
 197 bilinear interpolation.

198 For the evaluation of present-day extreme precipitation, we examined the maximum 1-day precipitation
 199 (Rx1d), maximum 1-hour precipitation (Rx1h), return-period-based precipitation amounts at 5, 10, 20, and 50-year
 200 return periods, frequency of daily precipitation exceeding 10, 15, 20 mm, and seasonality of frequency/intensity
 201 from regional to local scales. The calculation of seasonal Rx1d/Rx1h was based on the maximum value within one
 202 season per year.

203
 204

Table 1. The information for the ten hourly rain gauges.

Name	Station ID	Longitude (°E)	Latitude (°N)	Elevation	Region
Østre Toten - Apelsvoll	SN11500	10.8695	60.7002	264	Eastern
Ås - Rustadskogen	SN17870	10.8107	59.6703	120	Eastern
Kise in Hedmark	SN12550	10.8055	60.7733	128	Eastern
The Onion of Volbu	SN23500	9.063	61.122	521	Eastern
Kvithamar	SN69150	10.8795	63.4882	27	Middle-Coastal
Tjøtta	SN76530	12.4255	65.8295	21	Middle-Coastal
Stryn - The Hook	SN58900	6.5585	61.9157	208	Western
Fureneset	SN56420	5.0443	61.2928	7	Western
Særheim	SN44300	5.6508	58.7605	87	South-Western
Tromsø - Holt	SN90400	18.9095	69.6538	20	Northern-Coastal

205

206 3.2 Extreme precipitation indices

207 Generalized extreme value (GEV) distribution function was used to derive the precipitation at specified return
 208 periods (5, 10, 20, 50-year) from the statistical cumulative distribution functions of the conceptual distributions for
 209 the annual maximum precipitation derived from the precipitation series. GEV distribution has been widely used to
 210 model extreme events in meteorology (Coles et al., 2003). The cumulative distribution function $F(x)$ and
 211 probability density function $f(x)$ of GEV were as follows to calculate the return level Z_p :

212

$$213 \quad F(x) = \exp\left\{-\left[1 - k\left(\frac{x - \xi}{\alpha}\right)\right]^{1/k}\right\}, k \neq 0$$

$$214 \quad f(x) = \frac{1}{\alpha} \left[1 - k\left(\frac{x - \xi}{\alpha}\right)\right]^{1/k - 1} \exp\left\{-\left[1 - k\left(\frac{x - \xi}{\alpha}\right)\right]^{1/k}\right\}$$

$$215 \quad Z_p = \xi - \frac{\alpha}{k} \{1 - [-\log(1 - p)]^{-k}\}$$

216



217 Where, α , ξ , and k indicates the scale, location and shape parameter, respectively. Kolmogorov-Smirnovs,
218 Anderson-Darlings, and Chi-Square tests were performed to determine if the GEV was accepted to fit the maxima
219 series.
220

221 **3.3 Quantification of the orographic effect**

222 The orographic effect on Rx1h and Rx1d precipitation was explored by looking at the relationship with elevation of
223 the annual and seasonal maxima from regional to local scales. A linear regression model (Di Piazza et al., 2011) was
224 utilized to approximate the relations. The relation of elevation with observation (Rx1h: SeNorge2; Rx1d: SeNorge
225 and daily in-situ observation) and simulation (HCLIM3 and HCLIM12) was fitted to compute the linear regression
226 slopes and expressed as an averaged precipitation (mm) per kilometer of elevation. The orographic effect at local
227 scale was only based on daily in-situ observation due to the limited hourly in-situ observation. At local scale, the
228 elevation for each rain-gauges was extracted according to the digital elevation model. At regional scale, the grid of
229 digital elevation model and HCLIM3 was resample to the same grid resolution of 12 km as HCLIM12 before
230 calculation. Only the grids and stations above sea level of 0 m are included to quantify the orographic effect.

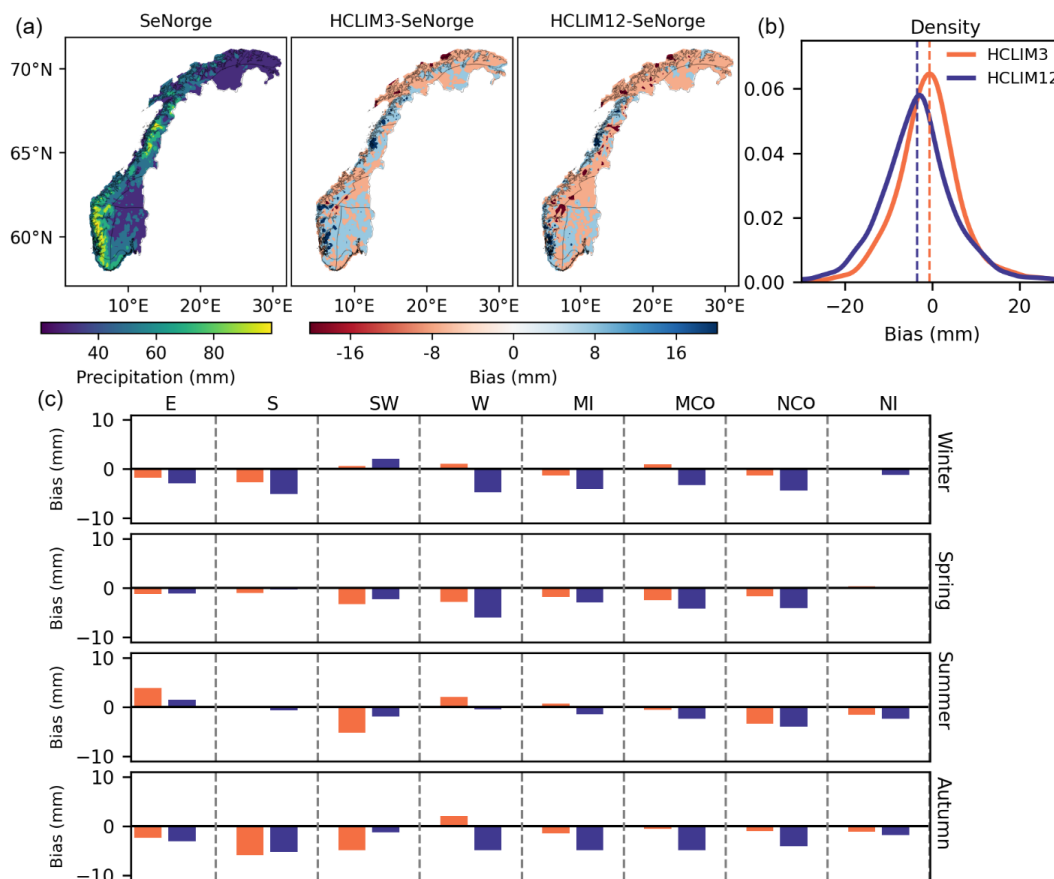
231 If the precipitation increases with elevation, it means that the orographic effect on extreme precipitation; if the
232 precipitation decreases with elevation, its means that the reverse orographic effect on extreme precipitation.
233

234 **4 Results**

235 **4.1 Evaluation of daily extreme with SeNorge**



236 **4.1.1 Rx1d precipitation**



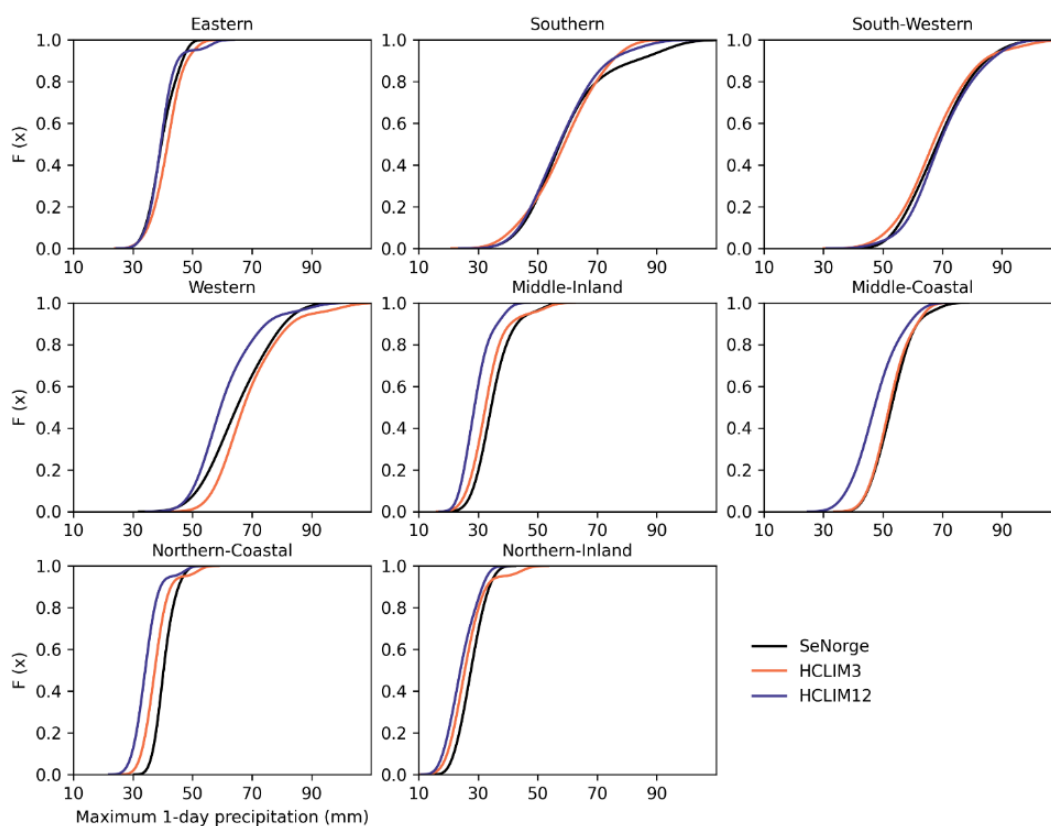
237
 238 **Figure 2: (a) Comparison of annual maximum 1-day precipitation (Rx1d) during 1999-2018; (b) density plot of the bias**
 239 **distribution from HCLIM3 and HCLIM12 compared to SeNorge for Rx1d during 1999-2018; (c) the bias of seasonal**
 240 **Rx1d from HCLIM3 and HCLIM12 to SeNorge for eight regions. For each region, the result is the bias is the average bias**
 241 **of grids within the region. The absolute differences are equal to model simulations minus observations, divided by**
 242 **observations.**

243
 244 Figure 2 provides a comprehensive comparison of Rx1d bias from HCLIM3 and HCLMI2 compared to SeNorge.
 245 From Fig. 2 (a), we can see that HCLIM12 has more grids with underestimated Rx1d than HCLMI3 in Norway,
 246 which is confirmed clearly in Fig. 2 (b) showing density plot of the bias distribution from two models compared
 247 with SeNorge. Specifically, more grids from HCLIM3 tend to overestimate Rx1d within the 0-10 mm/day range,
 248 while HCLIM12 leans towards underestimation. In addition, referred to Fig. S1, the spatial distribution of seasonal
 249 Rx1d is also shown. The density curve in Fig. 2 (b) reflects a higher peak at 0 for HCLIM3, indicating a more
 250 accurate representation of Rx1d with an average bias closer to 0. Conversely, HCLIM12 shows a dry-bias for Rx1d
 251 on average. Compared to the bias of annual precipitation in Fig. S2, we noted that HCLIM12 shows higher wet-bias
 252 for annual precipitation. This could be attributed to the overestimation of low-moderate precipitation (drizzle) in



253 HCLIM12, as suggested by Lind et al. (2020), who also highlighted the higher drizzle in HCLIM12, when comparing
254 the contribution of intense precipitation to total precipitation.

255 Figure 2 (c) shows the bias of Rx1d from HCLIM3 and HCLIM12 compared to SeNorge for eight regions in
256 four seasons. HCLIM3 better captures Rx1d in winter for all regions than HCLIM12, while HCLIM12 shows higher
257 dry-bias across regions except in the south-western region. In autumn, HCLIM3 shows more underestimation of
258 Rx1d in the southern and south-western regions but performs better elsewhere. Both HCLIM3 and HCLIM12 have
259 dry-bias for spring Rx1d in all regions except northern-inland with almost no-bias, and HCLIM12 has more
260 underestimation than HCLIM3 except in the southern and south-western regions. In summer, HCLIM3 outperforms
261 Rx1d in the 5 out of 8 over HCLIM12. Overall, HCLIM3 shows notably added value in Rx1d comparing with
262 HCLIM12 across regions and seasons although with exception of the south-western region.



263
264 **Figure 3: The empirical distribution of annual Rx1d during 1999-2018 in each of the eight Norway regions from SeNorge,**
265 **HCLIM3 and HCLIM12.**

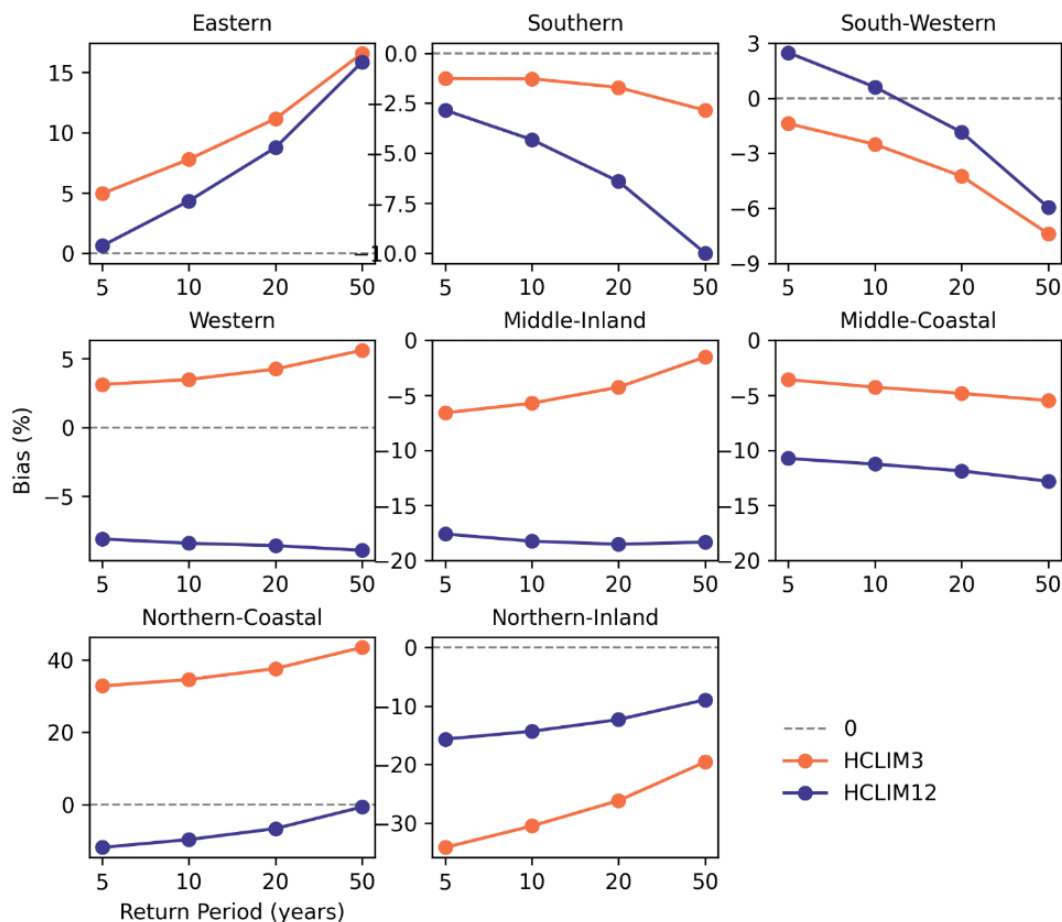
266
267 Furthermore, Fig. 3 shows the empirical distribution of Rx1d from HCLIM3 and HCLIM12 over all eight
268 regions during 1999-2018, compared to the SeNorge data. The distribution of Rx1d from HCLIM 3 and HCLIM12
269 varies among regions with intraregional differences. For example, Rx1d in the western region is overestimated by



270 HCLIM3, while underestimated by HCLIM12. Besides, both HCLIMs underestimate the Rx1d in the middle-inland,
 271 northern-coastal and northern-inland generally. HCLIM3 demonstrates overall closer alignment with SeNorge in
 272 four regions, specifically the western, middle-inland, middle-coastal and northern-coastal regions, compared to
 273 HCLIM12. In the eastern region, HCLIM3 tends to overestimate Rx1d when it is above 33.5 mm, while exhibits
 274 better performance when Rx1d is larger than 48.2 mm compared with HCLIM12. In contrast, in the northern-inland,
 275 HCLIM3 can better capture the Rx1d except the severe extremes. In the southern and south-western regions, the
 276 distributions from both HCLIMs are quite similar as SeNorge, posing challenges in discerning superiority.

277 **4.1.2 Return levels**

278



279

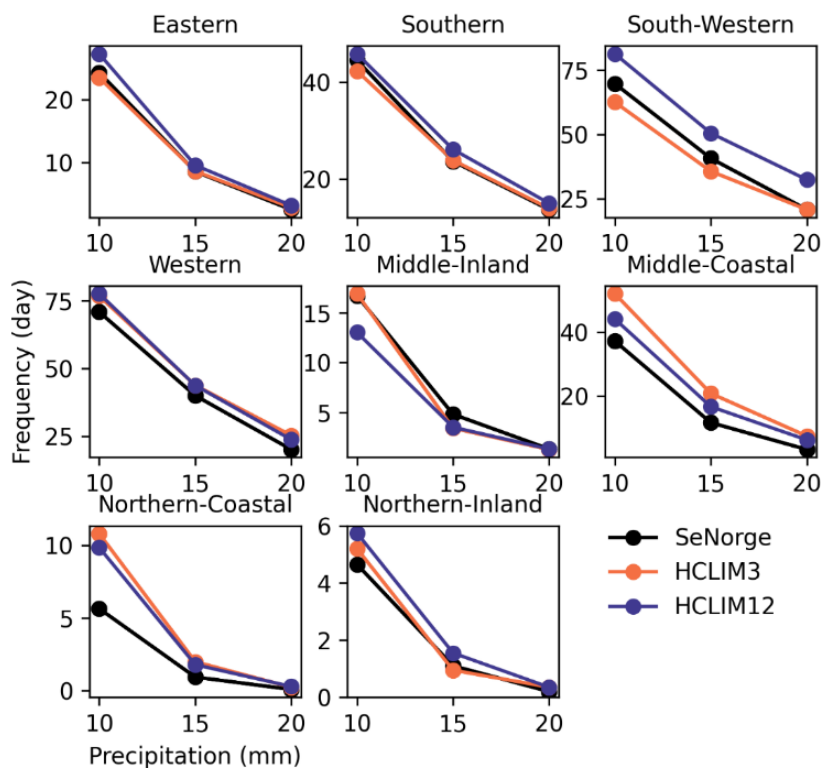
280 **Figure 4: The bias of extreme annual Rx1d exceeding the 5-year to 50-year over eight regions between seNorge and**
 281 **HCLIMs (i.e., HCLIM3 and HCLIM12).**

282

283



284



285

286 **Figure 5: The frequency of daily extreme precipitation exceeding 10, 15, 20mm/day.**

287

288 Figure 4 shows the bias in estimated daily precipitation for 5-, 10-, 20-, and 50-year return periods during 1999-2018
289 across eight regions (compared to SeNorge). The great interregional variation is shown between HCLIM3 and
290 HCLIM12. Relative to SeNorge, HCLIM3 tends to overestimate return-levels in the eastern, western and northern-
291 coastal regions, while underestimates them in the others. With the exception of the western and northern-coastal
292 regions, HCLIM12 shows a bias direction similar to HCLIM3. The performance of HCLIMs in capturing extremes
293 varies across regions. HCLIM3 consistently outperforms HCLIM12 in the southern, western, middle-inland and
294 middle-coastal regions for all return-periods, but performs less satisfactorily in other regions. As the return period
295 increases, the bias between HCLIMs and observations increases, except in the northern-inland region.

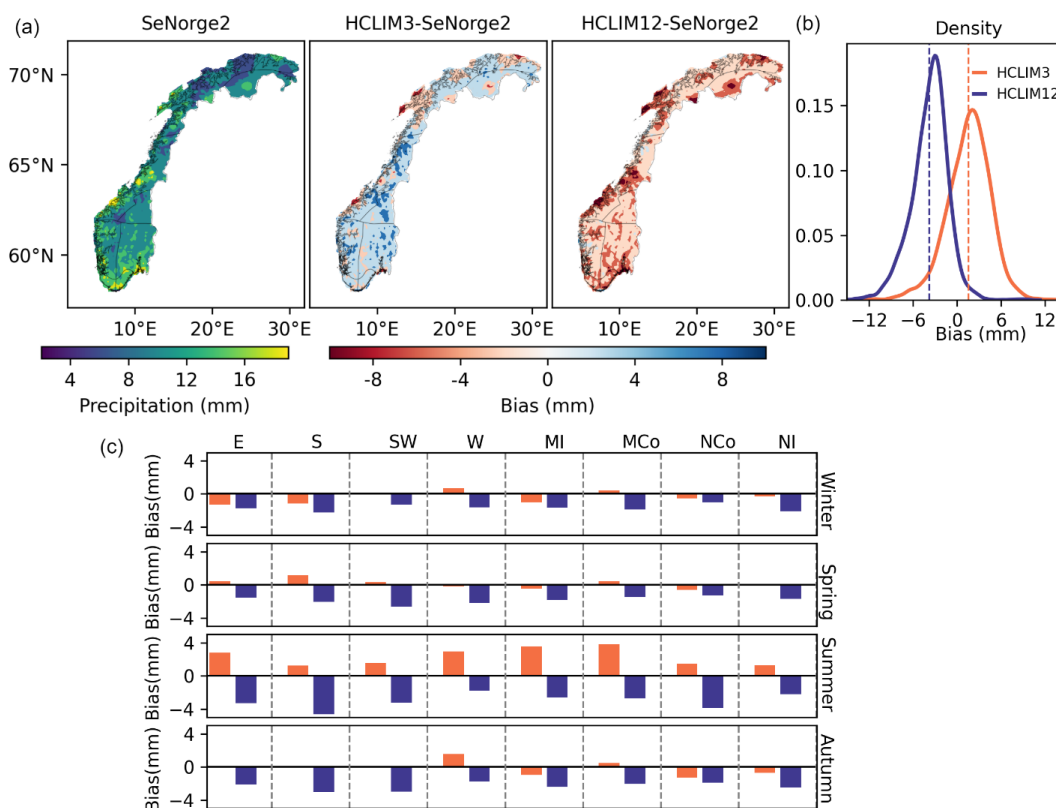
296 The frequency of precipitation exceeding 10, 15 and 20 mm is compared between simulations and observations
297 for eight regions in Fig. 5. The south-western and western regions experience frequent extreme precipitation events
298 exceeding 10, 15, and 20 mm/day. With exception in the western, middle-coastal and northern-coastal regions,
299 HCLIM3 can better capture the frequency of extreme precipitation than HCLIM12. HCLIM12 tends to overestimate
300 the frequency of extreme precipitation in most regions, except the middle-inland region. Both HCLIM3 and
301 HCLIM12 well capture the frequency as the severity of extremes increases.



302 Given the societal impacts of precipitation extremes, understanding how HCLIM3 and HCLIM12 represent
 303 these extremes is crucial. The physical processes driving precipitation in inland and coastal regions, as highlighted
 304 by Konstali and Sorteberg (2022), emphasize the need for a separate evaluation for each region with different
 305 characteristics. This approach ensures a more robust assessment, providing valuable information for regional
 306 authorities.

307 **4.1.3 Evaluation of hourly extreme with SeNorge2**

308



309

310 **Figure 6: (a) Comparison of annual Rx1h during 2010-2018; (b) density plot of bias distribution from HCLIM3 and**
 311 **HCLIM12 compared to SeNorge2 during 2010-2018; (c) the bias of seasonal Rx1h from HCLIM3 and HCLIM12 to**
 312 **SeNorge2 for eight regions. For each region, the result is the bias is the average bias of grids within the region.**

313

314 Figure 6 provides a comprehensive comparison of Rx1h bias from HCLIM3 and HCLMI12 comparing with
 315 SeNorge2 during 2010-2018. From Fig. 6 (a), we can see that HCLM3 overestimate the annual Rx1h, while
 316 HCLIM12 underestimate the Rx1h almost over Norway. Furthermore, the density plot of bias in Fig. 6 (b) showing
 317 the bias distribution from two models compared with SeNorge2, further confirmed the overestimation from
 318 HCLIM3 and underestimation from HCLIM12. On average, the annual Rx 1h in most grids could be better captured



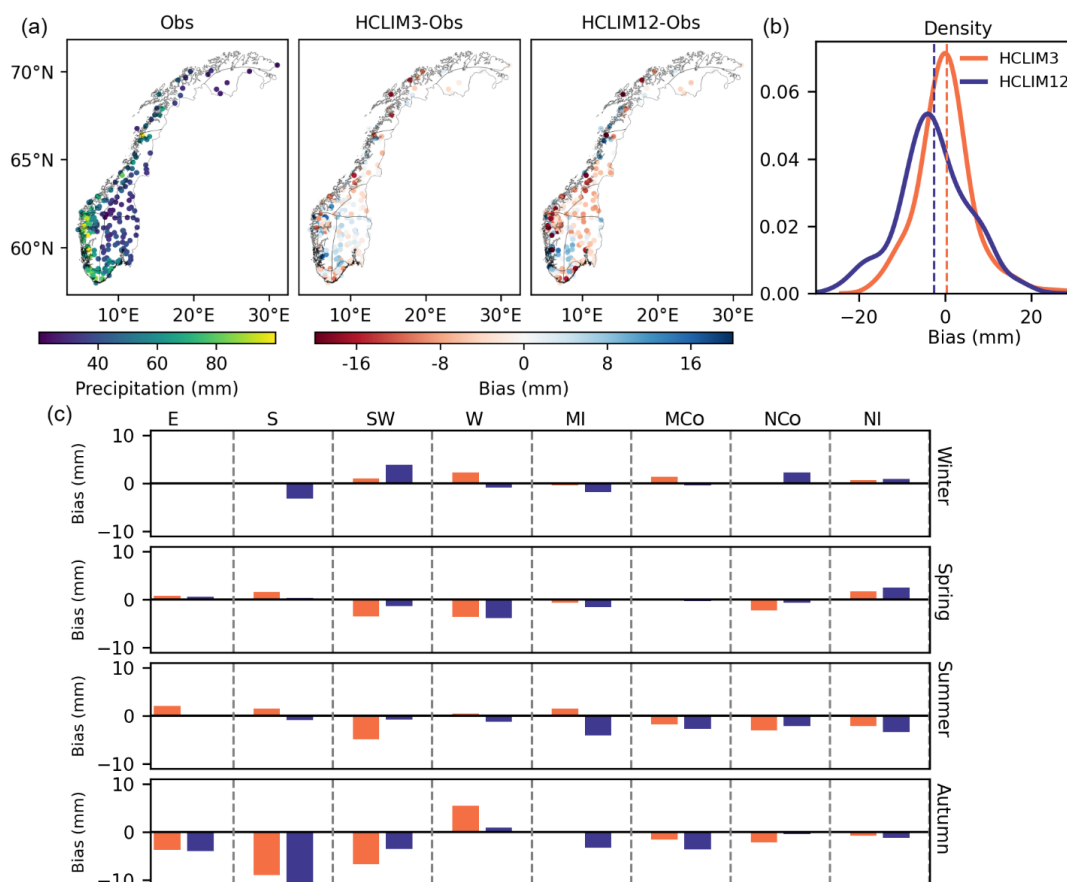
319 by HCLIM3 with an average bias (1.5 mm) closer to 0, than HCLIM12. Conversely, HCLIM12 underestimate Rx1h
 320 about 4 mm on average.

321 The bias of Rx1h from HCLIM3 and HCLIM12 compared to SeNorge2 for eight regions in four seasons is
 322 shown in Fig. 6 (c). HCLIM3 performs better in capturing seasonal Rx1h than HCLIM12 in most regions except
 323 western, middle-inland and middle-coastal regions during summer. Besides, the seasonal Rx1h except summer is
 324 better represented by HCLIM3 compared to HCLIM12. In summer, wet-bias in all region is observed from
 325 HCLIM3. HCLIM12 shows dry-bias in all regions and seasons.

326

327 4.2 Evaluation of daily extreme with in-situ data

328 4.2.1 Rx1d precipitation



329
 330 **Figure 7:** (a) The annual Rx1d of in-situ observation, and the bias of Rx1d from HCLIM3 and HCLIM12 to in-situ
 331 observation during 1999-2018 over 194 stations; (b) density distribution of Rx1d bias between HCLIMs and observations
 332 from 194 stations during 1999-2018; (c) the bias of seasonal Rx1d between HCLIMs and observations across the eight
 333 regions. For each region, it is the averaged bias from all stations in the region.

334



335 Similar to the regional results in Fig. 2, Fig. 7 shows the annual and seasonal bias of Rx1d from HCLIM3 and
336 HCLIM12 in comparison to in-situ observations. Notably, a larger difference between HCLIM3 and HCLIM12 can
337 be seen at local scale compared to regional result: a greater number of grids from HCLIM3 approach zero-bias, and
338 more grids from HCLIM12 shows a 20 mm dry bias, as shown in Fig. 7 (b). On average, HCLIM12 tends to
339 underestimate annual Rx1d, while HCLIM3 represents added value in capturing annual Rx1d at local scale.

340 When examined seasonally, as shown in Fig. 7 (c), excepting the western region with a wet bias, HCLIM3
341 shows better performance in capturing winter Rx1d. In spring, HCLIM12 falters in representing Rx1d in the
342 southern, south-western and northern-coastal regions, while HCLIM3 shows beneficial in most regions except the
343 south-western, western and northern-coastal regions during autumn. Notably, the performance of both HCLIM3 and
344 HCLIM12 at the local scale differs from the regional results. For example, their performance in the southern and
345 south-western regions during autumn deteriorates, displaying a more significant dry bias. In contrast, biases in the
346 eastern region from both HCLIM3 and HCLIM12 decrease in all seasons except winter.

347 Biases from HCLIM3 increase in the western region during winter, spring and autumn. HCLIM12 shows
348 improvement in capturing Rx1d at local scale compared to regional result except southern and south-western
349 regions. However, the benefit from HCLIM3 over HCLIM12 diminishes in the western region at local scale relative
350 to the regional scale. Notably, HCLIM3 fails to capture seasonal Rx1d in the south-western region, which is the
351 same as from the regional results. Therefore, HCLIM3 and HCLIM12 yield divergent outcomes across different
352 regions and seasons when examined at local scale compared to the regional scale.

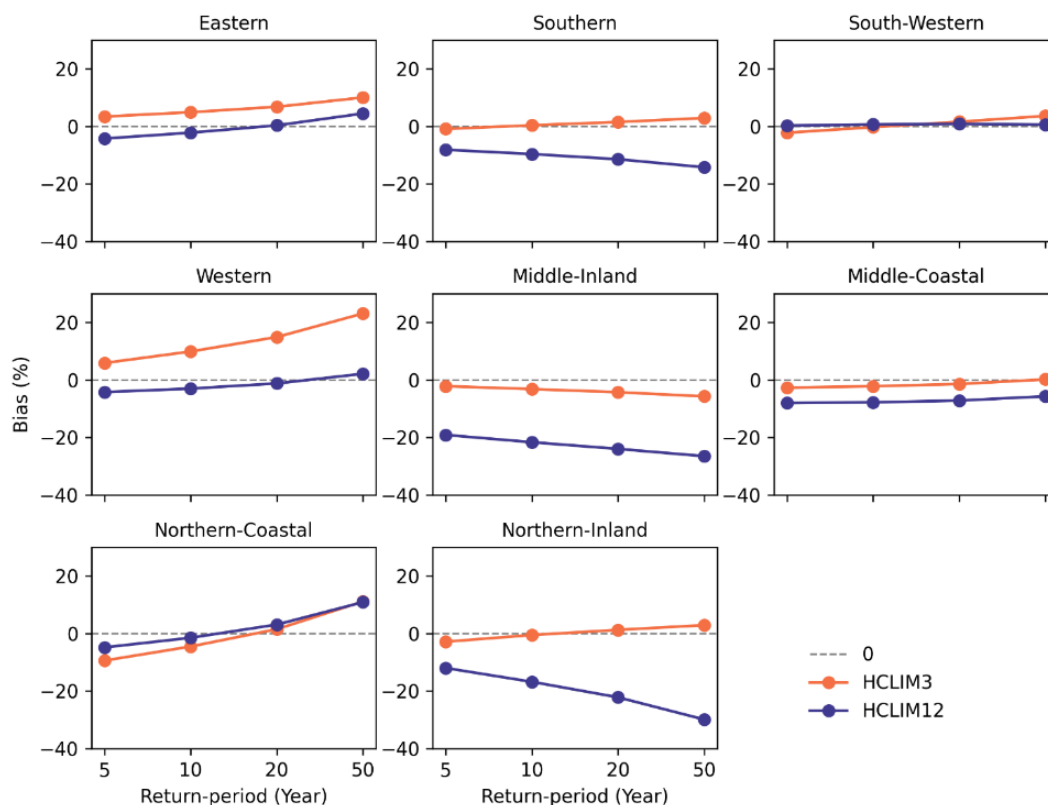
353



354

355 **4.2.2 Return-levels**

356



357

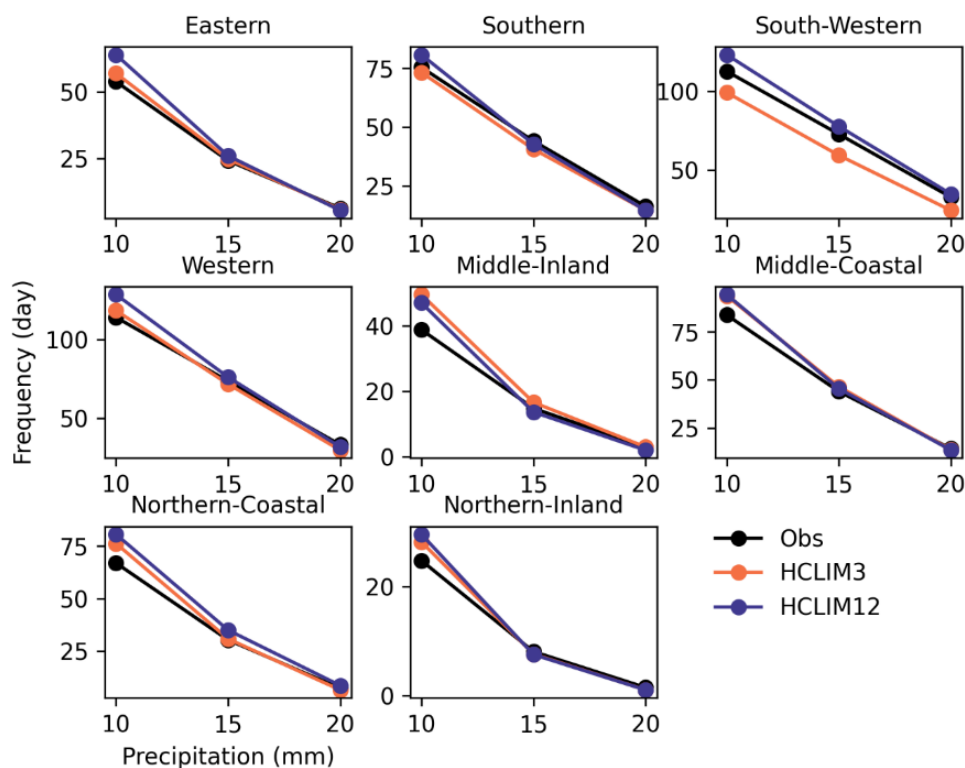
358 **Figure 8: Percentage biases of daily precipitation in the present-day for HCLIM3 and HCLIM12 relative to observation**
 359 **for 5-, 10-, 20-, and 50-year return periods in the 192 daily rain-gauges. Return periods of 5-, 10-, 20-, and 50-year are**
 360 **calculated on the basis of station-scale GEV. The bias of daily precipitation with different return-levels for each region is**
 361 **the averaged bias of all stations within the corresponding region.**

362

363 Figure 8 shows bias in estimating daily return levels (e.g., 5-, 10-, 20-, and 50-year return periods) from HCLIM3
 364 and HCLIM12 compared to observations during the 1999-2018. This figure illustrates the average bias for return-
 365 levels at grids within the corresponding regions. Biases from HCLIM3 and HCLIM12 exhibit variations across
 366 regions and return periods. HCLIM3 has a higher bias in the eastern, western and northern-coastal regions compared
 367 to HCLIM12, similar to the result at regional scale, while HCLIM12 shows larger uncertainty in the eastern region.
 368 Despite exceptions, HCLIM3 generally provides a more accurate representation of the return levels. Notably, in the
 369 northern-coastal, HCLIM3 exhibits lower bias for the return-level under 20-year return-period, but larger bias for the
 370 return-level under 5, 10, and 50-year return-periods. Both HCLIM3 and HCLIM12 perform well in the south-
 371 western region. In addition, the range of the return levels from all grids within the corresponding region is shown in



372 Fig. S3. In the western and northern-inland regions, HCLIM3 introduces larger uncertainty, as evident by a wider
 373 whisker, in comparison to HCLIM12. Additionally, with longer return periods, both the bias of extremes and its
 374 associated uncertainty estimated by HCLIMs tend to increase.
 375



376
 377 **Figure 9: The frequency of daily precipitation exceeding 10, 15, 20mm/day. The frequency for each region is the averaged**
 378 **frequency of all stations within the corresponding region.**

379 By comparing the frequency of extreme precipitation exceeding 10, 15, 20 mm/day from HCLIM3 and
 380 HCLIM12 to in-situ observation, as shown in Fig. 9, we find HCLIM3 outperforms HCLIM12 in capturing the
 381 frequency of extreme precipitation in the eight regions generally, except the south-western, middle-inland and
 382 middle-coastal regions. For the frequency of extreme precipitation above 20 mm/day, both HCLIMs capture it well.

383 Compared to the result in regional scale (Fig. 5), the frequency of daily extreme precipitation between regional
 384 scale and local scale is different. The frequency at local scale is higher than the regional scale across all regions.
 385 Besides, the intraregional difference for the added value of HCLIM3 is also different. For example, the added value
 386 of HCLIM3 is shown in the middle-coastal according to the regional result, while not shown according to local
 387 result. In general, the benefit of HCLIM3 in capturing the frequency of extreme precipitation is seen both in the
 388 regional and local scale.

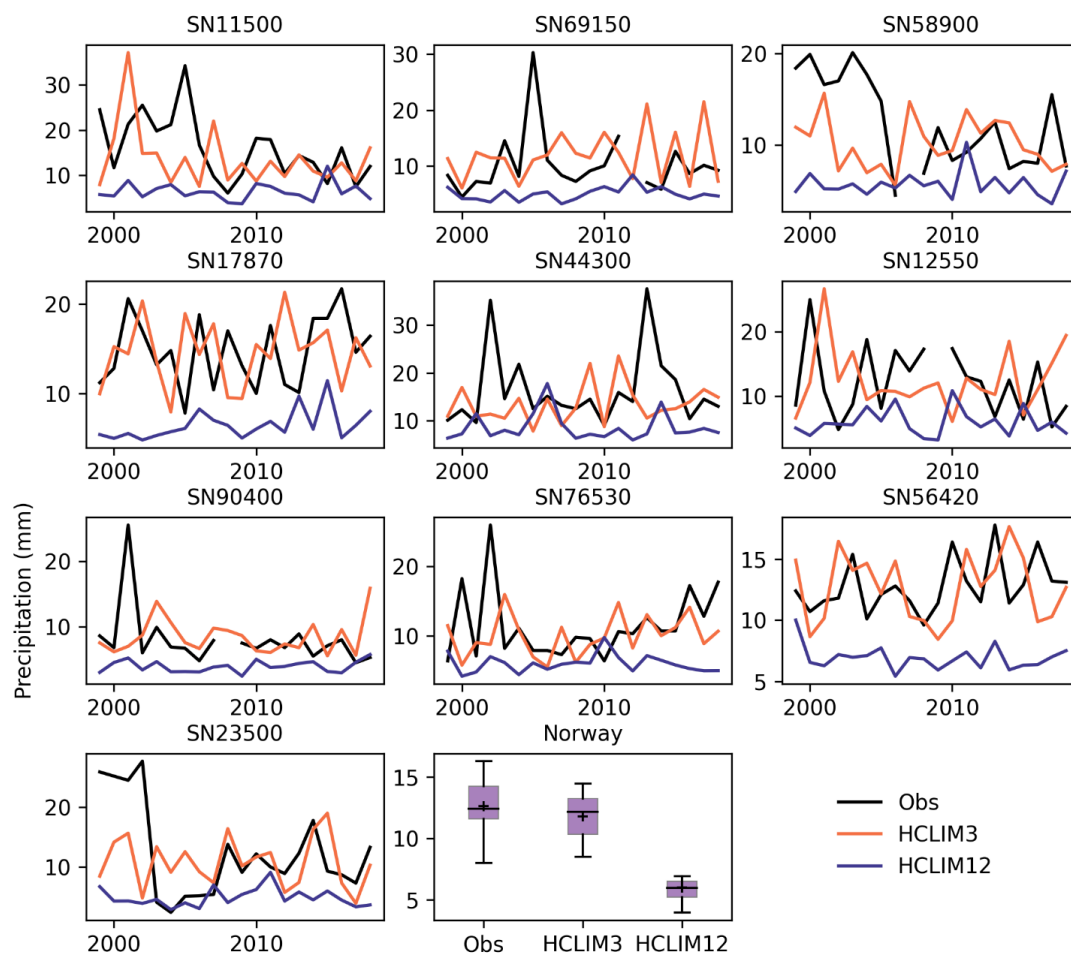
389
 390



391
 392
 393

394 **4.3 Evaluation of hourly extreme with in-situ data**

395 **4.3.1 Rx1h intensity**



396

397 **Figure 10: Time evolution of Rx1h precipitation for each year from observation, HCLIM3 and HCLIM12 during 1999-**
 398 **2018 at 10 rain-gauges.**

399

400 The time evolution of annual Rx1d from HCLIM3 and HCLIM12 is compared to in-situ observation during 1999-
 401 2018, as shown in Fig. 10. Compared to HCLIM12, HCLIM3 shows distinct superior in capturing the time evolution
 402 of annual Rx1d, even with underestimation and time shifting at some local places. For example, the annual Rx1d
 403 above 25 mm/day at SN69150, SN44300, SN90400, SN76530 and SN23500 is struggle to captured by HCLIM3 and
 404 HCLIM12. However, HCLIM3 well capture the annual Rx1d in other local places, despite of the time deviation of

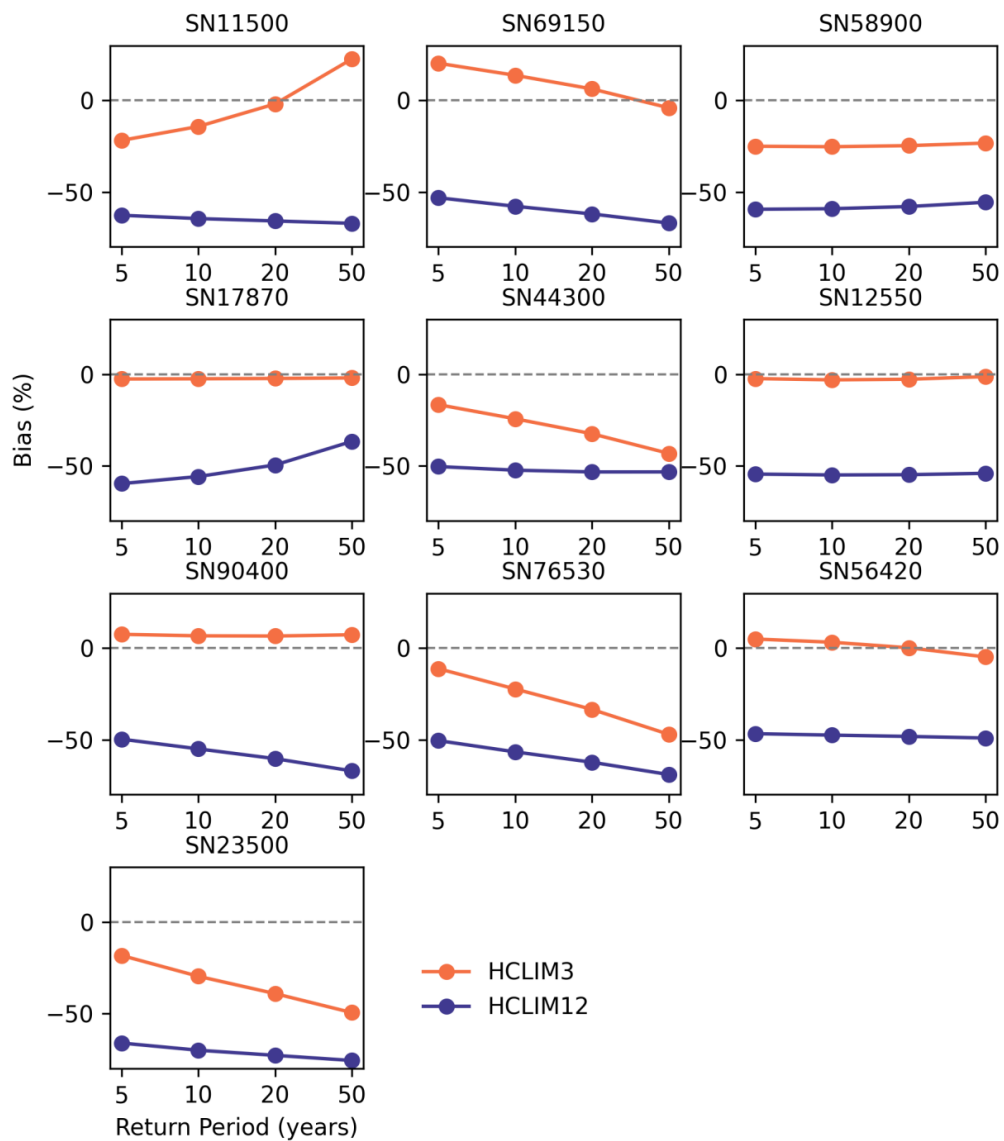


405 annual Rx1d. Taking the site SN11500 as an example to illustrate the time deviation: HCLIM3 simulate that the
406 annual Rx1d (37 mm) in the past 20 years was in 2001, four years earlier than the in-situ observation (35 mm).
407 Furthermore, to better assess the annual variability of Rx1h, we extracted grids within a 12 km radius of each station
408 and calculate the uncertainty range (Fig. S4). A comparison between HCLIM3 and HCLIM12 reveals that the
409 interpolated local Rx1h precipitation from HCLIM12, particularly over grids with a larger area, tends to be damped,
410 resulting in smaller return levels and a narrower range than HCLIM3. Importantly, the Rx1h in the past 20 years
411 (1999-2018) can be well captured by HCLIM3. In the view of station statistics for the mean annual Rx1d in Norway
412 (Fig.10) using boxplot, the mean annual Rx1d from HCLIM3 is within the range of observation, while HCLIM12 is
413 all below the minimum value of observation. Despite outperforming than HCLIM12, it is noteworthy that HCLIM3
414 demonstrates limitations in reproducing the accurate occurrence time and magnitude of annual Rx1h at local-level in
415 Norway.
416



417

418 4.3.2 Return levels

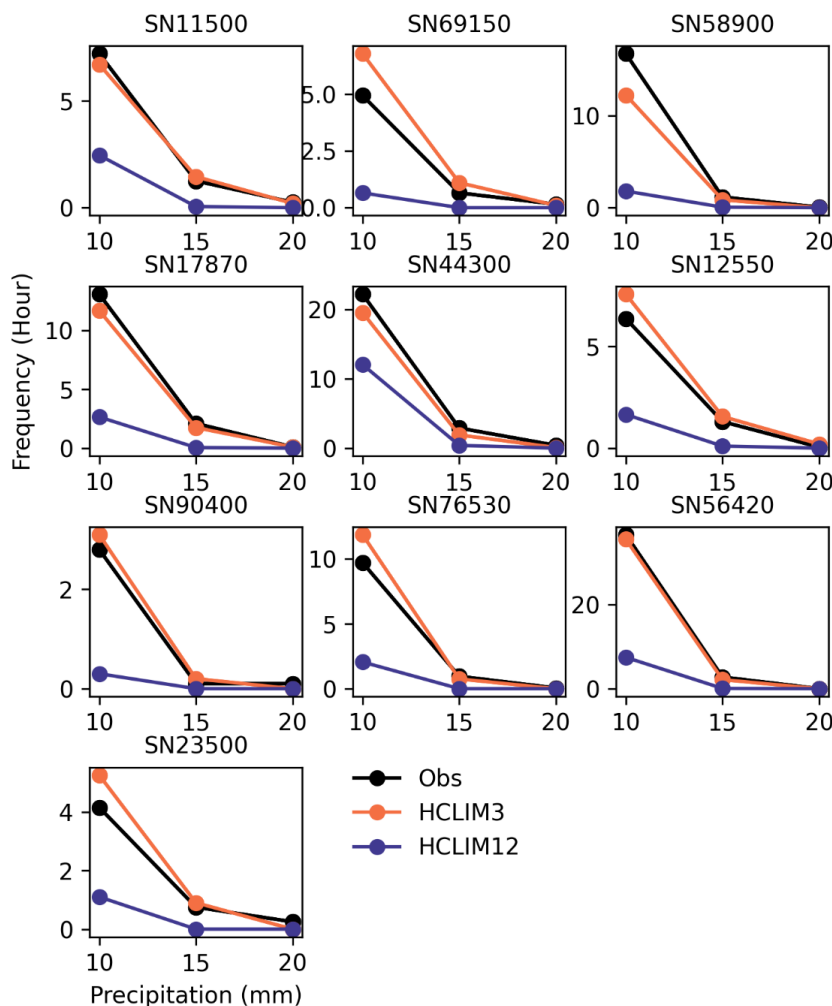


419

420 **Figure 11: The bias of Rx1h precipitation exceeds 5-year, 10-year, 20-year, and 50-year return levels between HCLIMs**
 421 **and in-situ observations (based on GEV method).**

422

423



424

425 **Figure 12: The frequency of hourly extreme precipitation exceeding 10, 15, 20mm from HCLIM3, HCLIM12 and in-situ**
 426 **observations.**

427

428 At the local and hourly scale, HCLIM3 has better representation of the frequency of hourly extreme events
 429 compared to HCLIM12. Despite both HCLIM3 and HCLIM12 underestimating the Rx1h precipitation for 5, 10, 20,
 430 and 50-year return periods at almost stations (Fig. 11), the bias for ten rain gauges between observations and
 431 interpolated HCLIM3 is consistently lower than that from HCLIM12 at all return periods. There is an exception, at
 432 SN11500, SN69150, SN90400 and SN56420, HCLIM3 shows slight overestimation. Moreover, the bias between
 433 HCLIMs and in-situ observation increased as return period increases. Notably, the return level of hourly extreme
 434 events at SN17870, SN12550, SN90400 and SN56420 is accurately captured by HCLIM3, indicating its ability to
 435 better capture the extreme hourly precipitation at 5,10,20,50-year return periods compared to HCLIM12 in localized



436 areas. This result shows the superiority of CPRCM in representing the frequency of extreme precipitation at a very
 437 localized scale, despite the underestimation of return levels from both HCLIM3 and HCLIM12.

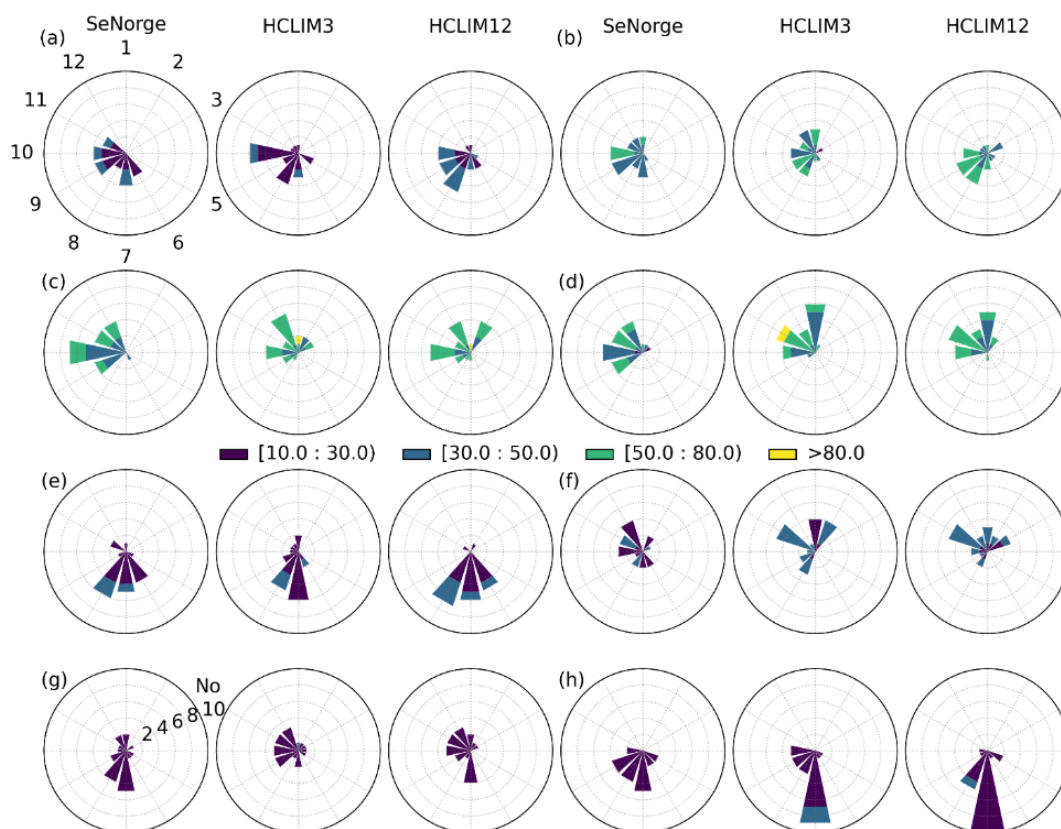
438 In addition, Fig. 12 shows the frequency of hourly precipitation exceeding 10, 15 and 20 mm at ten stations.
 439 The results further confirm the added value of CPRCM in capturing the frequency of extreme precipitation at very
 440 localized scale, despite the tendency to overestimate the frequency. This added value is more obvious than at the
 441 regional scale, although we acknowledge the uncertainty in the extreme precipitation analysis based on the
 442 stationary GEV method.

443

444 4.4 Evaluation of seasonality

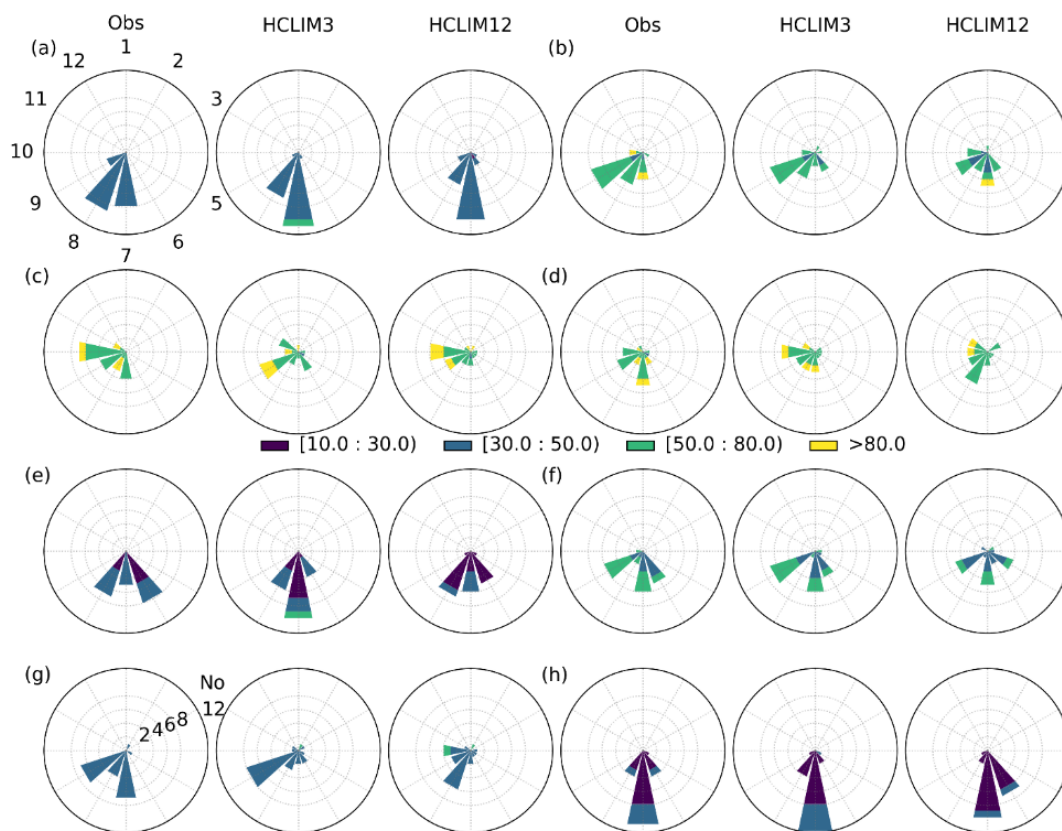
445

446



447

448 **Figure 13: The seasonality of frequency and magnitude of Rx1d precipitation from the SeNorge, HCLIM3 and HCLIM12**
 449 **during 1999-2018 over different regions: a) Eastern, b) Southern, c) South-Western, d) Western, e) Middle-Inland, f)**
 450 **Middle-Coastal, g) Northern-Coastal, h) Northern-Inland.**



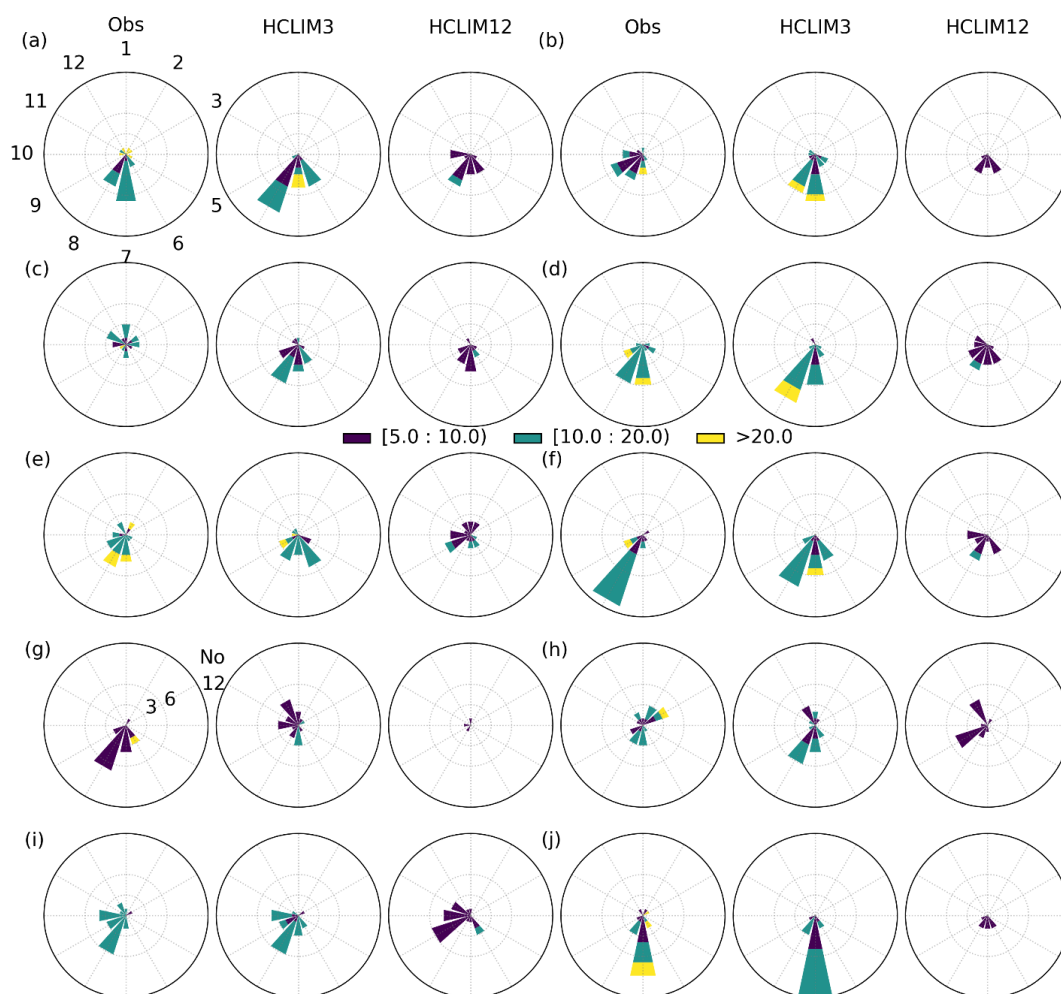
451

452 **Figure 14: The seasonality of frequency and magnitude of Rx1d precipitation from the in-situ observation, HCLIM3 and**
 453 **HCLIM12 during 1999-2018 over different regions: a) Eastern, b) Southern, c) South-Western, d) Western, e) Middle-**
 454 **Inland, f) Middle-Coastal, g) Northern-Coastal, h) Northern-Inland.**

455

456

457



458

459 **Figure 15: Seasonality of the frequency and magnitude of Rx1h precipitation from the in-situ, HCLIM3 and HCLIM12**
 460 **during 1999-2018 at 10 rain gauge stations (Table 1), i.e., a) SN11500, b) SN69150, c) SN58900, d) SN17870, e) SN44300, f)**
 461 **SN12550, g) SN90400, h) SN76530, i) SN56420, j) SN23500.**

462

463 Figure13 and Figure 14 show the comparison of seasonality (e.g., frequency and magnitude) of Rx1d from HCLIMs
 464 compared to SeNorge and in-situ observation, respectively. From the seasonality of daily extreme precipitation in
 465 Fig. 13, we can see that winter-autumn precipitation is dominant in almost all regions, except the Middle-Inland and
 466 Northern-Inland regions where spring-summer precipitation is dominant, similar results can be found in HCLIM3.
 467 However, the spring-summer dominant precipitation is observed in the Eastern region from HCLIM12. Heavy
 468 precipitation over 50 mm/day occurs mainly in the Southern, South-Western, and Western regions which is also
 469 simulated by both HCLIM3 and HCLIM12. In general, both HCLIM3 and HCLIM12 demonstrate competence in
 470 capturing the magnitude of extreme daily precipitation seasonally across all regions. Particularly noteworthy is the
 471 enhanced capability of HCLIM3 in capturing the seasonality of extreme precipitation frequency over the eastern,

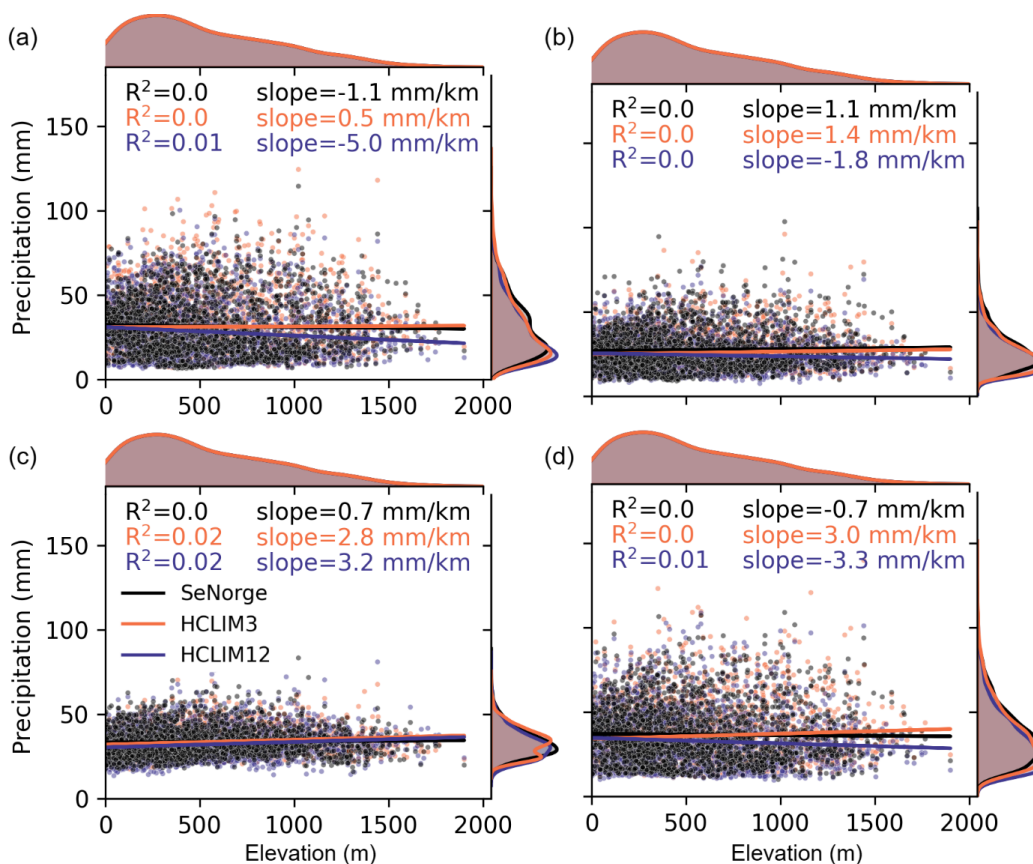


472 south-western, middle-inland, middle-coastal, and northern-coastal regions compared to HCLIM12. This superior
 473 representation of the frequency of extreme daily precipitation in HCLIM3 is consistently evident on a seasonal basis
 474 relative to HCLIM12. The performance of the seasonality of Rx1d from HCLIM3 and HCLIM12 in the regional
 475 scale is also confirmed by the in-situ observation (Fig. 14).

476 Examining the seasonality of Rx1h at local scale in Fig. 15, we can see that HCLIM3 provides a more accurate
 477 representation of the seasonality of Rx1h in comparison to HCLIM12, which fails to produce the Rx1h. However,
 478 comparing with in-situ observations, HCLIM3 tends to overestimate the frequency. For example, in SN58900 and
 479 SN56420 located in the Western region, HCLIM3 simulates more frequent events, although the magnitude of
 480 precipitation is underestimated. Both observations and HCLIM3 indicate that winter-autumn is dominant in the
 481 Western region. The CPRCM excels in reproducing the Rx1h, surpassing the RCM in both regional and station
 482 scales, particularly at localized scale.

483 4.5 Orographic effect on seasonal extreme precipitation

484 4.5.1 Seasonal Rx1d at regional scale



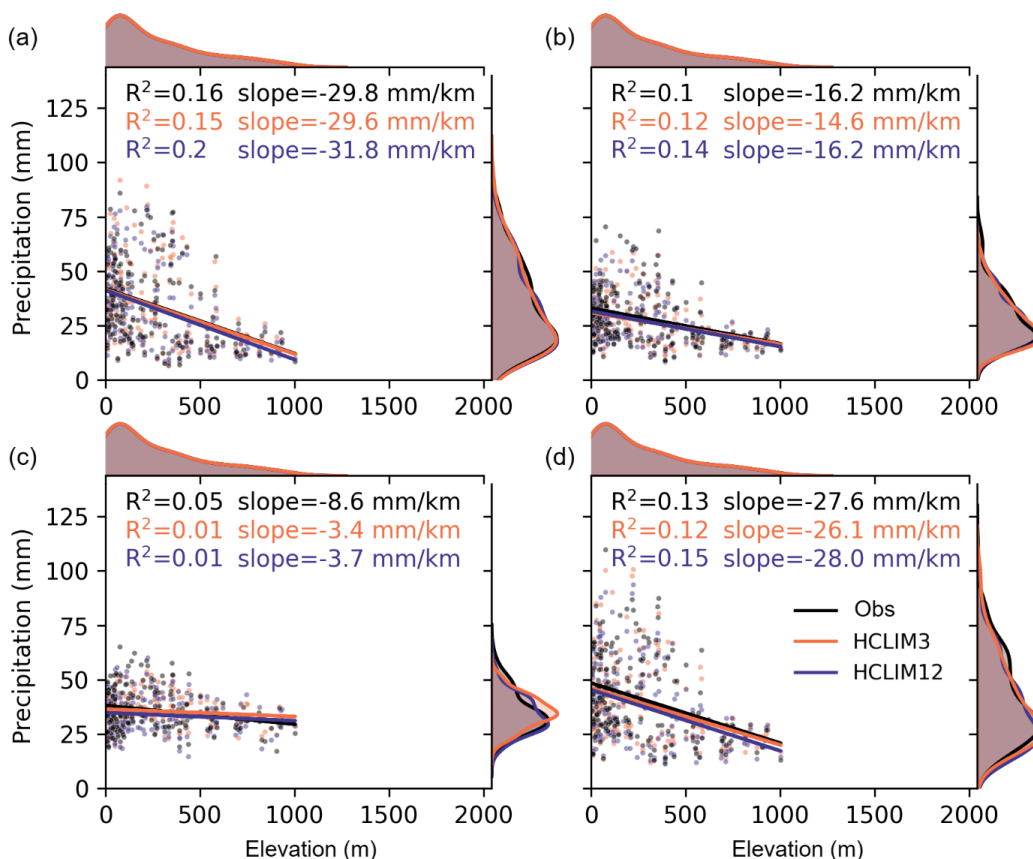
485
 486 Figure 16: Relation of (a) winter, (b) spring, (c) summer, and (d) autumn Rx1d from SeNorge and HCLIMs (i.e.,
 487 HCLIM3 and HCLIM12) with elevation over Norway between during 1999-2018.



488
489 The relationship of seasonal Rx1d with elevation from SeNorge, HCLIM3 and HCLIM12 is shown in Fig. 16. We
490 can see that HCLIM3 more accurately captures the no evident linear relation (indicated by zero coefficient of
491 determination) of seasonal Rx1d with elevation, similar to SeNorge, though it depicts a more pronounced increase
492 with elevation than SeNorge during summer. For example, both HCLIM3 and HCLIM12 simulate a large average
493 elevation-related increase in summer Rx1d (over 2.8 mm/km). Conversely, HCLIM12 reflects the reverse
494 orographic effect in winter and autumn Rx1d, showing a more significant decrease in Rx1d with elevation than
495 observation. The variation of Rx1d with elevation in HCLIM12 is consistently larger than observation, as indicated
496 by the larger absolute slope values.

497 4.5.2 Seasonal Rx1d at local scale

498



499

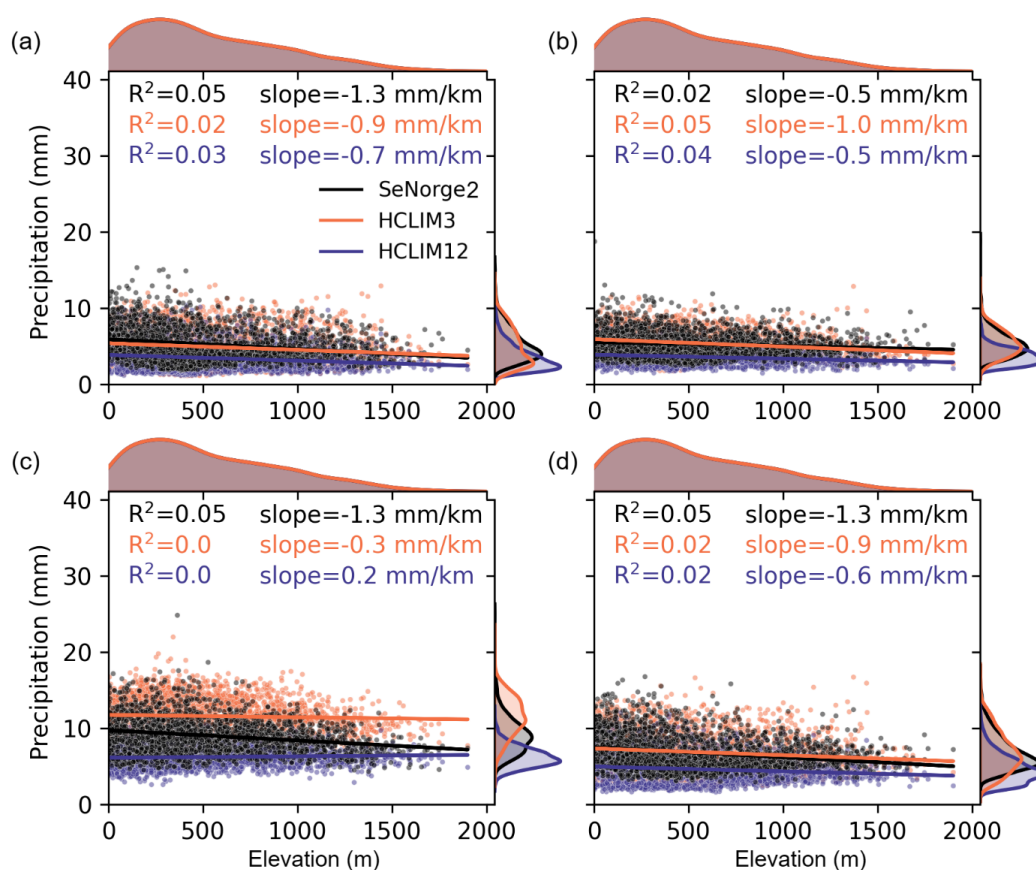
500 Figure 17: Relation of (a) winter, (b) spring, (c) summer, and (d) autumn Rx1d from daily in-situ observation and
501 HCLIMs (i.e., HCLIM3 and HCLIM12) with elevation over Norway between during 1999-2018.

502



503 Figure 17 represents the relationship of the seasonal Rx1d from in-situ observation, HCLIM3 and HCLIM12 with
504 elevation at local scale. The observed reverse orographic effect, seasonal Rx1d decrease with elevation, clearly
505 depicts with an average decrease of winter, spring, summer and autumn Rx1d of more than 29.8, 16.2, 8.6 and 27.6
506 mm/km. HCLIM3, although with smaller slope than observation, shows improvement in capturing the orographic
507 effect on winter Rx1d than HCLIM12. Moreover, HCLIM12 displays a more pronounced decline in Rx1d with
508 elevation, as evidenced by a steeper slope, across all seasons except summer, when compared to observation.
509 Despite of this, HCLIM12 more accurately represents the orographic influences on Rx1d in all seasons except
510 winter. Furthermore, as depicts in Fig. 17, the decreasing density of stations with increasing elevation complicates
511 the assessment of orography's impact, thereby challenging the reliability of our evaluations in elevated terrains.
512

513 4.5.3 Seasonal Rx1h at regional scale



514

515 Figure 18: Relation of (a) winter, (b) spring, (c) summer, and (d) autumn Rx1h from SeNorge2 and HCLIMs (i.e.,
516 HCLIM3 and HCLIM12) with elevation over Norway between during 2010-2018.

517



518 The relationship of seasonal Rx1h with elevation from gridded observation and simulation is further explored, as
519 shown in Fig. 18. Different with seasonal Rx1d at regional scale, the reverse orography effect on Rx1h from
520 SeNorge2 clearly emerges in all seasons, with an average decrease of more than 1.3, 0.5, 1.3 and 1.3 mm/km in
521 winter, spring, summer and autumn, respectively. HCLIM3 more accurately captures the pronounced decrease in
522 seasonal Rx1h with elevation during winter, summer and autumn, though it still underestimates the decrease relative
523 to actual observation. By contrast, HCLIM12 can only reflect the similar reverse orographic on Rx1h with
524 observation in spring. The density plots of Rx1h reveal a significant dry bias in HCLIM12, particularly noticeable in
525 summer, where it inversely correlates Rx1h with elevation. HCLIM3 more effectively represents the reverse
526 orographic impact on hourly precipitation than on daily, as seen by comparing the slope and precipitation
527 distribution in the Fig. 16 and Fig. 18.
528

529 **5 Discussion**

530 **5.1 Added value of CPRCM at regional scale**

531 The comparison between HCLIM3 and HCLIM12 reveals distinct biases in the representation of Rx1d, particularly
532 marked by an orographic effect. HCLIM3, on average, exhibits lower bias compared to HCLIM12, with notable
533 overestimation of precipitation along coastal areas. Converse to the wet-bias from HCLIM3, HCLIM12 shows
534 underestimation in the complex orography for the annual Rx1d. This discrepancy is attributed to unrealistic cloud
535 concentration nuclei numbers, while complex terrain areas also experience overestimation of precipitation from
536 HCLIM3 due to micro-physics, confirming findings from Lind et al. (2020). The comparison in Fig. S2 for annual
537 precipitation also represents large difference, particularly marked by a coastal-mountain-inland division. HCLIM3,
538 on average, exhibits a slightly larger wet-bias compared to HCLIM12 over the complex terrain, which could be
539 related to the model physics confirmed by Lind et al. (2020).

540 Notably, CPRCM (i.e., HCLIM3) demonstrates more significant benefits in capturing Rx1d at numerous grids
541 in Norway compared to SeNorge. Spatial variations in precipitation patterns across eight regions in Norway further
542 highlight the nuanced performance of HCLIM3, particularly in complex topography areas. Consistent with the
543 observation from Dyrødal et al. (2015), HCLIM3 also displays a lower bias than HCLIM12 on average, aligning
544 with the observed strong west-east gradient of precipitation over complex terrain. Dyrødal et al. (2015) and Poujol
545 et al. (2021) emphasize the diverse mechanisms driving precipitation in different regions of Norway. For instance,
546 extreme precipitation in the western region is dominated by frontal systems and orography during autumn and
547 winter, while convective activity plays a crucial role in the southern regions during summer (Li et al., 2020b).
548 HCLIM3, however, slightly overestimates annual Rx1d in complex terrain, indicating challenges in convection
549 parameterization schemes.

550 The study by Thomassen et al. (2023) utilizing SPHEAR with a 2.2 km resolution echoes challenges in
551 accurately simulating extreme precipitation over complex terrain in the northern Italy. Our findings confirm the



552 benefit of convection-permitting models in capturing spatial distribution in complex terrain, even though slight
553 positive biases persist when compared with SeNorge data.

554 A potential reason for the observed biases is related to the limitations of pseudo-observation SeNorge, which
555 may inadequately represent steep valleys at the 3 km grid space (Thomassen et al., 2023). Sparse station distribution
556 in complex mountain areas may contribute to unrealistic observations, concealing the benefits from HCLIM3. The
557 future work should delve into biases introduced by SeNorge and its potential impact on observed precipitation
558 patterns. Comparisons between SeNorge and HCLIM3 in data-sparse areas should be approached with caution due
559 to uncertainties associated with the SeNorge dataset.

560 The comparison of HCLIM3 and HCLIM12 in terms of seasonal Rx1d reveals better representation by
561 HCLIM3, except for a dry bias in the southwest region. This dry bias could be attributed to the limitations of
562 HCLIM3 in capturing specific precipitation mechanisms in this region.

563 Furthermore, HCLIM3 shows obvious benefit in capturing Rx1h on average than HCLIM12, even with wet-
564 bias from HCLIM3 compared to hourly SeNorge2 over Norway. Most grids from HCLIM12 underestimate the
565 Rx1h, indicating the misrepresentation from parameterization schemes, confirming the finding from Lind et al.
566 (2020), more “drizzle” in HCLIM12. The uniformed spatial variation for the annual Rx1h may be attributed to the
567 too sparse station distribution (Lind et al., 2020), resulting in the damping for local storms. The station density
568 induced error from gridded dataset has also been indicated in Gervais et al. (2014b), who suggested the source for
569 large errors in gridded dataset when station density is low.

570 In summary, HCLIM3 demonstrates better agreement with observations at regional scales in Norway
571 compared to HCLIM12. This is consistent with previous studies highlighting the superiority of convection-
572 permitting models, especially in capturing extreme precipitation events over complex terrain.

573

574 **5.2 Added value of CPRCM at local scale**

575 The examination of CPRCM at the local scale reveals its superiority representation of extreme precipitation. Our
576 analysis focuses on in-situ observations (at local scale), recognizing the limitations of aggregation, regional average
577 or pooling techniques at grid scale, as highlighted by Kendon et al. (2023).

578 Chapman et al. (2023) compared return-levels between an Africa convection-permitting climate model with
579 4.5 km grid-spacing (CP4A) and observation at station-level and grid and found large differences. CP4A closely
580 aligns with station return-levels but exhibits a slight undercatch for the precipitation. Our results at station scale
581 corroborates these results, as return levels consistently underestimate extreme precipitation in HCLIM3. In line with
582 findings in Malawi, where regional-climate-model (P25) overestimated return levels with increasing return periods.
583 The damped extremes from averaged precipitation within the gridbox may cause smaller return-level at grid scale.
584 Therefore, significant bias of HCLIM3 and HCLIM12 relative to observation between local scale (station-level) and
585 regional scale may also be attributed to the damped extremes. The hourly and daily precipitation extremes from
586 HCLIM3 at most stations show more realistic results than at the regional scale, supporting the hypothesis of damped
587 extremes at regional scale weakening the superior, even though more bias is observed than regional result.



588 Despite the higher uncertainty associated with extremes from CPRCM at local scale (Chan et al., 2020;
589 Cannon et al., 2019), our results demonstrate smaller biases in HCLIM3. The higher extreme damping in HCLIM12,
590 averaging over coarse resolutions (~12km), may contribute to its higher dry bias. Furthermore, the credibility of
591 CPRCM in providing reliable representation for extremes may attribute to resolve deeply convective activities at
592 sub-grid scale, while the deficiency in the convection-parameterization scheme (HCLIM12) may bring uncertainty.
593 In contrast to the numerical instability in RCMs noted by Kendon et al. (2023), we note underestimation of
594 extremes, including return-level and time evolution in HCLIM12 at local scale, attributable to its convection-
595 parameterization scheme. In summary, the added value of HCLIM3 in capturing the frequency of extreme
596 precipitation at station scales, especially at highly localized local scale, is evident when compared to HCLIM12.

597 Few studies have compared sub-daily and daily rainfall in RCMs due to its unreliable prediction at sub-daily
598 scale. Following Ban et al. (2014), we recognize that the added value of CPRCM in capturing sub-daily or daily
599 precipitation extremes is different. The performance of RCM ~10 km in representing sub-daily rainfall was limited,
600 which has been proved hard to capturing sub-daily extreme rainfall in the southwestern United States (Jiang et al.,
601 2013).

602 Contrary to sub-daily extremes, HCLIM12 demonstrates higher merit in capturing daily extreme precipitation,
603 with biases less than 50%. By comparing the Rx1d/Rx1h at local scale, we also note that the added value of
604 HCLIM3 in capturing the Rx1h is more obvious. The superior performance at hourly scale is consistent with
605 findings by Médus et al. (2022) and Ban et al. (2014), emphasizing the significantly better sub-daily precipitation
606 characteristics of CPRCM, including spatial distribution and duration-intensity features.

607 **5.3 Seasonality of extreme precipitation**

608 The performance of CPRCM in capturing the seasonality of precipitation driven by different physical process has
609 been a subject of investigation in previous studies. Moustakis et al. (2021) highlighted the adequacy of CPRCM
610 (CTL-WRF~4 km) in capturing observed seasonality in the United States. Prein et al. (2013) also emphasized
611 CPRCM's ability to better reflect summer precipitation due to stronger deep convective activity. They found there
612 was less difference between RCM and CPRCM in capturing winter precipitation.

613 In our comparison between HCLIM12 and HCLIM3, we observe superior representation of hourly
614 precipitation seasonality in HCLIM3. The frequency and intensity of Rx1d in regional scale and Rx1h at station-
615 level can be better captured by HCLIM3, especially for local scale. The varying response to seasonal extreme
616 precipitation across different regions with distinct climate characteristics suggests that CPRCM tends to perform
617 better in specific regions or seasons with more convective precipitation. This aligns with finding from Prein et al.
618 (2013), emphasizing CPRCM's strength in capturing convective processes.

619 Further investigation of CPRCM and RCM performance in different regions regarding extreme precipitation
620 reveals the added value of HCLIM3, especially when assessing precipitation frequency and intensity on a seasonal
621 basis. This advantage is more pronounced at the local scale compared to the regional scale. However, investigating
622 daily precipitation intensify and frequency at local scale reveals unexpected results, notably the intensify of Rx1d
623 during winter is better captured, while the southern and south-western regions with more convective activity during



624 summer are poorly represented by HCLIM3. This suggests that HCLIM3's performance is not solely constrained by
625 specified convective precipitation, and the consistent underestimation of Rx1d intensity during summer in
626 HCLIM12 may be attributed to higher uncertainty from its convective parameterization scheme or numerical
627 uncertainties at the local scale.

628 **5.4 Added value of CPRCM in reproducing orographic effect**

629 At the local scale, seasonal Rx1d decrease with elevation, known as reverse orographic effect, is captured by
630 HCLIMs in all seasons. Compared to HCLIM12, HCLIM3 shows added value in representation of reverse
631 orographic effect during winter. In other seasons, however, HCLIM12 shows more improvement in the relation of
632 extreme precipitation with elevation than HCLIM3. It is noteworthy that the differences in how seasonal Rx1d
633 relates to elevation are more pronounced at a regional scale than at a local scale.

634 At regional scale, no evident relation of Rx1d with elevation is found from observation in all seasons, which
635 have also been shown from HCLIMs except summer. Furthermore, the unclear relation of seasonal Rx1d with
636 elevation at regional scale was also seen from the study of Dallan et al. (2023), in which, they analyzed annual Rx1d
637 based on CPRCMs and in-situ observation over Alpine. In summer, HCLIMs show the orographic effect on Rx1d,
638 which may be explained by the overestimated orographic precipitation from HCLIMs. Different to the unclear
639 orographic impact on Rx1d at regional scale, steeper slope is clearly seen than that from the local scale. Conversely,
640 the so-called "orographic enhancement" (Avanzi et al., 2021), precipitation increase on the windward side induced
641 by the lifting of air masses, and decrease along the leeward side due to air descent and drying is not found here at the
642 regional or local scales.

643 For hourly extremes, the results of reverse orography effect on seasonal Rx1h are consistent with previous
644 study of Dallan et al. (2023), which also found the weak decrease of annual Rx1d from CPRCMs to elevation than
645 in-situ observation over Alpine. HCLIM3 and HCLIM12 well capture the reverse orography effect on Rx1h,
646 especially in HCLIM3, although a stronger decrease of Rx1h with elevation is observed from SeNorge2 except
647 spring. Besides, lower Rx1h and weak reverse orography effect is found in HCLIM12 in all seasons. The orographic
648 effect on hourly and daily extremes seasonally suggests the influence of orography on extreme precipitation at
649 different timescales, and highlights the reliable simulation of extreme precipitation over complex orography. Our
650 findings confirm the reverse orographic effect on Rx1h, as previously observed for hourly precipitation (Marra et al.,
651 2021).

652 In summer, the poor performance from HCLIM3 and HCLIM12 in capturing orography effect and extreme
653 precipitation may be related to the intense orographically-sustained convection affected by atmospheric, aerosol
654 conditions, local terrain slope and shadowing effects, which failed to be captured by 3 km CPRCMs (Dallan et al.,
655 2023; Poujol et al., 2021). Moreover, Marra et al. (2021) also confirmed that the reverse orography effect on short-
656 duration precipitation extremes could be attributed to a weakening of updrafts of moist air over mountain ridge by
657 orographic turbulence. However, another major source resulting in the bias between HCLIMs and observation could
658 be related to the observation uncertainty. Sparseness of hourly stations and undercatch problems could also lead to



659 underestimation and underestimation of precipitation, especially in the complex orography (Lussana et al., 2018,
660 2019).

661 Furthermore, we acknowledged that the linear regression method is closely related to the distribution of data
662 point. More specifically, the different relationship between seasonal Rx1d and elevation may be attributed to the
663 uncertainty from the observed data. For example, there is limited rain gauges over the complex orography, the
664 highest rain-gauges are located about 1000 m. Importantly, several land surface characteristics could influence the
665 precipitation, a multiple linear regression model should be considered to quantify the orographic effect more realism
666 (Zhang et al., 2018). Besides, there might be uncertainty from SeNorge gridded dataset. Therefore, the relationship
667 between Rx1d and elevation remains inconclusive. Besides, the reverse orographic effect from Rx1h also needs to
668 be improved due to the lack of sufficiently long data records. Enhanced observation and more comprehensive
669 datasets are necessary to solidify our understanding of this connection.

670

671 **6 Conclusions**

672 In this study, we conducted a comprehensive evaluation of extreme precipitation characteristics from regional to
673 local scale in Norway, focusing on eight distinct regions, utilizing a convection-permitting regional climate model
674 (HCLIM3) and comparing it with its convection-parameterized regional climate model (HCLIM12) forced by ERA-
675 Interim data during 1999-2018.

676 The key conclusions drawn from this study are as follows:

- 677 a) For daily extreme precipitation at regional scale, HCLIM3 shows benefit in capturing Rx1d compared to
678 HCLIM12, showcasing improved representation of Rx1d in all seasons in the most of regions except
679 south-western. The added value of HCLIM3 varies across regions, demonstrating its superiority in
680 capturing return levels and daily extreme precipitation frequency, particularly in the southern, middle-
681 inland, middle-coastal, and northern-inland regions based on both SeNorge and in-situ data. HCLIM3
682 shows greater potential in reproducing the frequency of daily extreme precipitation exceeding 10, 15, and
683 20 mm.
- 684 b) For hourly extreme precipitation at regional scale, HCLIM3 also shows superiority on average, with wet-
685 bias based on SeNorge2, compared to HCLIM12. Furthermore, the added value from HCLIM3 in
686 capturing seasonal Rx1h is also observed than HCLIM12 in all seasons and regions except western,
687 middle-inland and middle-coastal regions during summer. In contrast, the overestimation of Rx1h from
688 HCLIM12 across eight regions in Norway is found.
- 689 c) For daily extreme precipitation at local scale, the Rx1d feature including frequency, intensity and return
690 level in most regions can be better captured by HCLIM3 than HCLIM12, although the benefit from
691 HCLIM3 over HCLIM12 diminishes in western region at local scale compared to that at regional scale.
692 Except south-western, HCLIM3 also have not superiority in capturing Rx1d in the western region.
- 693 d) For hourly extreme precipitation at the local scale, HCLIM3 outperforms HCLIM12 in capturing the
694 annual variability of Rx1h during 1999-2018, although the shifting of peak occurrence or magnitude is



695 observed than observation at some stations. Compared to HCLIM12, the add-value of HCLIM3 in
696 capturing Rx1h is more obvious at local scale than regional scale. The extreme precipitation characteristics
697 including frequency, intensity and return-level from HCLIM2 at local scale are underestimated seriously.
698 Besides, HCLIM3 also shows more added value in capturing Rx1h than Rx1d from regional to local scale.
699 e) For the seasonality of extremes, our analysis reveals no substantial difference between HCLIM3 and
700 HCLIM12 when it comes to daily extremes. However, a distinct advantage emerges with HCLIM3 for
701 hourly extremes, where it accurately reflects both the occurrence and intensity of these events across
702 different seasons. On the other hand, HCLIM12 tends to underestimate these aspects, demonstrating a
703 significant bias in capturing the frequency and magnitude of hourly extreme
704 f) The reserve orographic effect on seasonal Rx1h at regional scale emerge in Norway and can be better
705 captured by HCLIM3 than HCLIM12 except spring, although a stronger decrease is found in observation.
706 Additionally, a significant reverse orographic effect on seasonal Rx1d at the local scale has been observed,
707 with HCLIM3 providing added value, especially in capturing winter Rx1d. However, the relationship
708 between seasonal Rx1d and elevation at the regional scale remains ambiguous.
709

710 Acknowledgments

711 We would like to thank Stefan P. Sobolowski and Ozan Mert Gokturk, for their great supports as PI and data
712 manager of the EU Impetus4change (I4C) project, respectively. This research was supported by the European
713 Union's Horizon 2020 research, innovation programme under grant agreement no. 101081555
714 (IMPETUS4CHANGE) and the Research Council of Norway through FRINATEK Project 274310. The computer
715 resources were available through the RCN's program for supercomputing (NOTUR/NORSTORE); projects
716 NN10014K and NS10014K. All simulation data in this paper are available from the authors upon request
717 (luli@norceresearch.no).

718

719 *Competing interests.* The authors declare that they have no conflict of interest.

720 References

721 Adinolfi, M., Raffa, M., Reder, A., and Mercogliano, P.: Evaluation and Expected Changes of Summer Precipitation
722 at Convection Permitting Scale with COSMO-CLM over Alpine Space, 10.3390/atmos12010054, 2021.
723 Avanzi, F., Ercolani, G., Gabellani, S., Cremonese, E., Pogliotti, P., Filippa, G., Morra di Cella, U., Ratto, S.,
724 Stevenin, H., Cauduro, M., and Juglair, S.: Learning about precipitation lapse rates from snow course data
725 improves water balance modeling, *Hydrol. Earth Syst. Sci.*, 25, 2109-2131, 10.5194/hess-25-2109-2021,
726 2021.



- 727 Ban, N., Schmidli, J., and Schär, C.: Evaluation of the convection-resolving regional climate modeling approach in
728 decade-long simulations, *Journal of Geophysical Research: Atmospheres*, 119, 7889-7907,
729 <https://doi.org/10.1002/2014JD021478>, 2014.
- 730 Ban, N., Rajczak, J., Schmidli, J., and Schär, C.: Analysis of Alpine precipitation extremes using generalized
731 extreme value theory in convection-resolving climate simulations, *Climate Dynamics*, 55, 61-75,
732 [10.1007/s00382-018-4339-4](https://doi.org/10.1007/s00382-018-4339-4), 2020.
- 733 Benedict, I., Ødemark, K., Nipen, T., and Moore, R.: Large-Scale Flow Patterns Associated with Extreme
734 Precipitation and Atmospheric Rivers over Norway, *Monthly Weather Review*, 147, 1415-1428,
735 <https://doi.org/10.1175/MWR-D-18-0362.1>, 2019.
- 736 Cannon, A. J. and Innocenti, S.: Projected intensification of sub-daily and daily rainfall extremes in convection-
737 permitting climate model simulations over North America: implications for future intensity–duration–
738 frequency curves, *Nat. Hazards Earth Syst. Sci.*, 19, 421-440, [10.5194/nhess-19-421-2019](https://doi.org/10.5194/nhess-19-421-2019), 2019.
- 739 Chan, S. C., Kendon, E. J., Berthou, S., Fosser, G., Lewis, E., and Fowler, H. J.: Europe-wide precipitation
740 projections at convection permitting scale with the Unified Model, *Clim Dyn*, 55, 409-428,
741 [10.1007/s00382-020-05192-8](https://doi.org/10.1007/s00382-020-05192-8), 2020.
- 742 Chapman, S., Bacon, J., Birch, C. E., Pope, E., Marsham, J. H., Msemo, H., Nkonde, E., Sinachikupo, K., and
743 Vanya, C.: Climate Change Impacts on Extreme Rainfall in Eastern Africa in a Convection-Permitting
744 Climate Model, *Journal of Climate*, 36, 93-109, <https://doi.org/10.1175/JCLI-D-21-0851.1>, 2023.
- 745 Coles, S., Pericchi, L. R., and Sisson, S.: A fully probabilistic approach to extreme rainfall modeling, *Journal of*
746 *Hydrology*, 273, 35-50, [https://doi.org/10.1016/S0022-1694\(02\)00353-0](https://doi.org/10.1016/S0022-1694(02)00353-0), 2003.
- 747 Dallan, E., Marra, F., Fosser, G., Marani, M., Formetta, G., Schär, C., and Borga, M.: How well does a convection-
748 permitting regional climate model represent the reverse orographic effect of extreme hourly precipitation?,
749 *Hydrol. Earth Syst. Sci.*, 27, 1133-1149, [10.5194/hess-27-1133-2023](https://doi.org/10.5194/hess-27-1133-2023), 2023.
- 750 Di Piazza, A., Conti, F. L., Noto, L. V., Viola, F., and La Loggia, G.: Comparative analysis of different techniques
751 for spatial interpolation of rainfall data to create a serially complete monthly time series of precipitation for
752 Sicily, Italy, *International Journal of Applied Earth Observation and Geoinformation*, 13, 396-408,
753 <https://doi.org/10.1016/j.jag.2011.01.005>, 2011.
- 754 Dyrørdal, A. V.: Estimating extreme precipitation on different spatial and temporal scales in Norway, PhD thesis,
755 Faculty of Mathematics and Natural Sciences, University of Oslo, Oslo, Norway, 96 pp., 2015.
- 756 Dyrørdal, A. V., Médus, E., Dobler, A., Hodnebrog, Ø., Arnbjerg-Nielsen, K., Olsson, J., Thomassen, E. D., Lind, P.,
757 Gaile, D., and Post, P.: Changes in design precipitation over the Nordic-Baltic region as given by
758 convection-permitting climate simulations, *Weather and Climate Extremes*, 42, 100604,
759 [10.1016/j.wace.2023.100604](https://doi.org/10.1016/j.wace.2023.100604), 2023.
- 760 Gervais, M., Gyakum, J. R., Atallah, E., Tremblay, L. B., and Neale, R. B.: How Well Are the Distribution and
761 Extreme Values of Daily Precipitation over North America Represented in the Community Climate System
762 Model? A Comparison to Reanalysis, Satellite, and Gridded Station Data, *Journal of Climate*, 27, 5219-
763 5239, <https://doi.org/10.1175/JCLI-D-13-00320.1>, 2014a.



- 764 Gervais, M., Tremblay, L. B., Gyakum, J. R., and Atallah, E.: Representing Extremes in a Daily Gridded
765 Precipitation Analysis over the United States: Impacts of Station Density, Resolution, and Gridding
766 Methods, *Journal of Climate*, 27, 5201-5218, <https://doi.org/10.1175/JCLI-D-13-00319.1>, 2014b.
- 767 Giordani, A., Cerenzia, I. M. L., Paccagnella, T., and Di Sabatino, S.: SPHERA, a new convection-permitting
768 regional reanalysis over Italy: Improving the description of heavy rainfall, *Quarterly Journal of the Royal
769 Meteorological Society*, 149, 781-808, <https://doi.org/10.1002/qj.4428>, 2023.
- 770 Jiang, P., Gautam, M. R., Zhu, J., and Yu, Z.: How well do the GCMs/RCMs capture the multi-scale temporal
771 variability of precipitation in the Southwestern United States?, *Journal of Hydrology*, 479, 75-85,
772 <https://doi.org/10.1016/j.jhydrol.2012.11.041>, 2013.
- 773 Kendon, E. J., Fischer, E. M., and Short, C. J.: Variability conceals emerging trend in 100yr projections of UK local
774 hourly rainfall extremes, *Nature Communications*, 14, 1133, [10.1038/s41467-023-36499-9](https://doi.org/10.1038/s41467-023-36499-9), 2023.
- 775 Kendon, E. J., Stratton, R. A., Tucker, S., Marsham, J. H., Berthou, S., Rowell, D. P., and Senior, C. A.: Enhanced
776 future changes in wet and dry extremes over Africa at convection-permitting scale, *Nature
777 Communications*, 10, 1794, [10.1038/s41467-019-09776-9](https://doi.org/10.1038/s41467-019-09776-9), 2019.
- 778 Kent, C., Dunstone, N., Tucker, S., Scaife, A. A., Brown, S., Kendon, E. J., Smith, D., McLean, L., and Greenwood,
779 S.: Estimating unprecedented extremes in UK summer daily rainfall, *Environmental Research Letters*, 17,
780 014041, [10.1088/1748-9326/ac42fb](https://doi.org/10.1088/1748-9326/ac42fb), 2022.
- 781 Kim, Y., Rocheta, E., Evans, J. P., and Sharma, A.: Impact of bias correction of regional climate model boundary
782 conditions on the simulation of precipitation extremes, *Climate Dynamics*, 55, 3507-3526, [10.1007/s00382-
783 020-05462-5](https://doi.org/10.1007/s00382-020-05462-5), 2020.
- 784 Knist, S., Goergen, K., and Simmer, C.: Evaluation and projected changes of precipitation statistics in convection-
785 permitting WRF climate simulations over Central Europe, *Climate Dynamics*, 55, 325-341,
786 [10.1007/s00382-018-4147-x](https://doi.org/10.1007/s00382-018-4147-x), 2020.
- 787 Konstali, K. and Sorteberg, A.: Why has Precipitation Increased in the Last 120 Years in Norway?, *Journal of
788 Geophysical Research: Atmospheres*, 127, [10.1029/2021jd036234](https://doi.org/10.1029/2021jd036234), 2022.
- 789 Li, J., Gan, T. Y., Chen, Y. D., Gu, X., Hu, Z., Zhou, Q., and Lai, Y.: Tackling resolution mismatch of precipitation
790 extremes from gridded GCMs and site-scale observations: Implication to assessment and future projection,
791 *Atmospheric Research*, 239, 104908, <https://doi.org/10.1016/j.atmosres.2020.104908>, 2020a.
- 792 Li, L., Pontoppidan, M., Sobolowski, S., and Senatore, A.: The impact of initial conditions on convection-permitting
793 simulations of a flood event over complex mountainous terrain, *Hydrol. Earth Syst. Sci.*, 24, 771-791,
794 [10.5194/hess-24-771-2020](https://doi.org/10.5194/hess-24-771-2020), 2020b.
- 795 Li, P., Furtado, K., Zhou, T., Chen, H., and Li, J.: Convection-permitting modelling improves simulated
796 precipitation over the central and eastern Tibetan Plateau, *Quarterly Journal of the Royal Meteorological
797 Society*, 147, 341-362, <https://doi.org/10.1002/qj.3921>, 2021.
- 798 Lind, P., Lindstedt, D., Kjellström, E., and Jones, C.: Spatial and Temporal Characteristics of Summer Precipitation
799 over Central Europe in a Suite of High-Resolution Climate Models, *Journal of Climate*, 29, 3501-3518,
800 <https://doi.org/10.1175/JCLI-D-15-0463.1>, 2016.



- 801 Lind, P., Belušić, D., Christensen, O. B., Dobler, A., Kjellström, E., Landgren, O., Lindstedt, D., Matte, D.,
802 Pedersen, R. A., Toivonen, E., and Wang, F.: Benefits and added value of convection-permitting climate
803 modeling over Fenno-Scandinavia, *Climate Dynamics*, 55, 1893-1912, 10.1007/s00382-020-05359-3,
804 2020.
- 805 Liu, C., Ikeda, K., Rasmussen, R., Barlage, M., Newman, A. J., Prein, A. F., Chen, F., Chen, L., Clark, M., Dai, A.,
806 Dudhia, J., Eidhammer, T., Gochis, D., Gutmann, E., Kurkute, S., Li, Y., Thompson, G., and Yates, D.:
807 Continental-scale convection-permitting modeling of the current and future climate of North America,
808 *Climate Dynamics*, 49, 71-95, 10.1007/s00382-016-3327-9, 2017.
- 809 Lussana, C., Tveito, O. E., Dobler, A., and Tunheim, K.: seNorge_2018, daily precipitation, and temperature
810 datasets over Norway, *Earth Syst. Sci. Data*, 11, 1531-1551, 10.5194/essd-11-1531-2019, 2019.
- 811 Lussana, C., Saloranta, T., Skaugen, T., Magnusson, J., Tveito, O. E., and Andersen, J.: seNorge2 daily
812 precipitation, an observational gridded dataset over Norway from 1957 to the present day, *Earth Syst. Sci.*
813 *Data*, 10, 235-249, 10.5194/essd-10-235-2018, 2018.
- 814 Mahoney, K., Ralph, F. M., Wolter, K., Doesken, N., Dettinger, M., Gottas, D., Coleman, T., and White, A.:
815 Climatology of Extreme Daily Precipitation in Colorado and Its Diverse Spatial and Seasonal Variability,
816 *Journal of Hydrometeorology*, 16, 781-792, <https://doi.org/10.1175/JHM-D-14-0112.1>, 2015.
- 817 Marra, F., Armon, M., Borga, M., and Morin, E.: Orographic Effect on Extreme Precipitation Statistics Peaks at
818 Hourly Time Scales, *Geophysical Research Letters*, 48, e2020GL091498,
819 <https://doi.org/10.1029/2020GL091498>, 2021.
- 820 Médus, E., Thomassen, E. D., Belušić, D., Lind, P., Berg, P., Christensen, J. H., Christensen, O. B., Dobler, A.,
821 Kjellström, E., Olsson, J., and Yang, W.: Characteristics of precipitation extremes over the Nordic region:
822 added value of convection-permitting modeling, *Nat. Hazards Earth Syst. Sci.*, 22, 693-711, 10.5194/nhess-
823 22-693-2022, 2022.
- 824 Michel, C., Sorteberg, A., Eckhardt, S., Weijenberg, C., Stohl, A., and Cassiani, M.: Characterization of the
825 atmospheric environment during extreme precipitation events associated with atmospheric rivers in Norway
826 - Seasonal and regional aspects, *Weather and Climate Extremes*, 34, 100370, 10.1016/j.wace.2021.100370,
827 2021.
- 828 Moustakis, Y., Papalexiou, S. M., Onof, C. J., and Paschalis, A.: Seasonality, Intensity, and Duration of Rainfall
829 Extremes Change in a Warmer Climate, *Earth's Future*, 9, e2020EF001824,
830 <https://doi.org/10.1029/2020EF001824>, 2021.
- 831 Piani, C., Weedon, G. P., Best, M., Gomes, S. M., Viterbo, P., Hagemann, S., and Haerter, J. O.: Statistical bias
832 correction of global simulated daily precipitation and temperature for the application of hydrological
833 models, *Journal of Hydrology*, 395, 199-215, <https://doi.org/10.1016/j.jhydrol.2010.10.024>, 2010.
- 834 Pontoppidan, M., Kolstad, E. W., Sobolowski, S., and King, M. P.: Improving the Reliability and Added Value of
835 Dynamical Downscaling via Correction of Large-Scale Errors: A Norwegian Perspective, *Journal of*
836 *Geophysical Research: Atmospheres*, 123, 11,875-811,888, 10.1029/2018jd028372, 2018.



- 837 Poujol, B., Mooney, P. A., and Sobolowski, S. P.: Physical processes driving intensification of future precipitation
838 in the mid- to high latitudes, *Environmental Research Letters*, 16, 034051, 10.1088/1748-9326/abdd5b,
839 2021.
- 840 Prein, A. F., Holland, G. J., Rasmussen, R. M., Done, J., Ikeda, K., Clark, M. P., and Liu, C. H.: Importance of
841 Regional Climate Model Grid Spacing for the Simulation of Heavy Precipitation in the Colorado
842 Headwaters, *Journal of Climate*, 26, 4848-4857, <https://doi.org/10.1175/JCLI-D-12-00727.1>, 2013.
- 843 Prein, A. F., Langhans, W., Fosser, G., Ferrone, A., Ban, N., Goergen, K., Keller, M., Tölle, M., Gutjahr, O., Feser,
844 F., Brisson, E., Kollet, S., Schmidli, J., van Lipzig, N. P. M., and Leung, R.: A review on regional
845 convection-permitting climate modeling: Demonstrations, prospects, and challenges, *Reviews of*
846 *Geophysics*, 53, 323-361, <https://doi.org/10.1002/2014RG000475>, 2015.
- 847 Reder, A., Raffa, M., Montesarchio, M., and Mercogliano, P.: Performance evaluation of regional climate model
848 simulations at different spatial and temporal scales over the complex orography area of the Alpine region,
849 *Natural Hazards*, 102, 151-177, 10.1007/s11069-020-03916-x, 2020.
- 850 Rossi, M. W., Anderson, R. S., Anderson, S. P., and Tucker, G. E.: Orographic Controls on Subdaily Rainfall
851 Statistics and Flood Frequency in the Colorado Front Range, USA, *Geophysical Research Letters*, 47,
852 e2019GL085086, <https://doi.org/10.1029/2019GL085086>, 2020.
- 853 Schaller, N., Sillmann, J., Müller, M., Haarsma, R., Hazeleger, W., Hegdahl, T. J., Kelder, T., van den Oord, G.,
854 Weerts, A., and Whan, K.: The role of spatial and temporal model resolution in a flood event storyline
855 approach in western Norway, *Weather and Climate Extremes*, 29, 100259,
856 <https://doi.org/10.1016/j.wace.2020.100259>, 2020.
- 857 Tabari, H.: Climate change impact on flood and extreme precipitation increases with water availability, *Scientific*
858 *Reports*, 10, 13768, 10.1038/s41598-020-70816-2, 2020.
- 859 Thackeray, C. W., Hall, A., Norris, J., and Chen, D.: Constraining the increased frequency of global precipitation
860 extremes under warming, *Nature Climate Change*, 12, 441-448, 10.1038/s41558-022-01329-1, 2022.
- 861 Thomassen, E. D., Arnbjerg-Nielsen, K., Sørup, H. J. D., Langen, P. L., Olsson, J., Pedersen, R. A., and
862 Christensen, O. B.: Spatial and temporal characteristics of extreme rainfall: Added benefits with sub-
863 kilometre-resolution climate model simulations?, *Quarterly Journal of the Royal Meteorological Society*,
864 149, 1913-1931, <https://doi.org/10.1002/qj.4488>, 2023.
- 865 Wang, Y., Zhang, G. J., and He, Y.-J.: Simulation of Precipitation Extremes Using a Stochastic Convective
866 Parameterization in the NCAR CAM5 Under Different Resolutions, *Journal of Geophysical Research:*
867 *Atmospheres*, 122, 12,875-812,891, <https://doi.org/10.1002/2017JD026901>, 2017.
- 868 Zhang, T., Li, B., Yuan, Y., Gao, X., Sun, Q., Xu, L., and Jiang, Y.: Spatial downscaling of TRMM precipitation
869 data considering the impacts of macro-geographical factors and local elevation in the Three-River
870 Headwaters Region, *Remote Sensing of Environment*, 215, 109-127,
871 <https://doi.org/10.1016/j.rse.2018.06.004>, 2018.



872 Vormoor, K., Lawrence, D., Schlichting, L., Wilson, D., and Wong, W. K.: Evidence for changes in the magnitude
873 and frequency of observed rainfall vs. snowmelt driven floods in Norway, *Journal of Hydrology*, 538, 33-
874 48, 10.1016/j.jhydrol.2016.03.066, 2016.
875